HHS Public Access

Author manuscript

Cell Rep. Author manuscript; available in PMC 2020 September 28.

Published in final edited form as:

Cell Rep. 2020 September 08; 32(10): 108119. doi:10.1016/j.celrep.2020.108119.

Cholinergic Synaptic Homeostasis Is Tuned by an NFAT-Mediated α7 nAChR-K_V4/Shal Coupled Regulatory System

Abdunaser Eadaim[1], **Eu-Teum Hahm**[1], **Elizabeth D. Justice**[1], **Susan Tsunoda**[1,2,*]

[1]Department of Biomedical Sciences, Colorado State University, Fort Collins, CO 80523, USA

[2]Lead Contact

SUMMARY

Homeostatic synaptic plasticity (HSP) involves compensatory mechanisms employed by neurons and circuits to preserve signaling when confronted with global changes in activity that may occur during physiological and pathological conditions. Cholinergic neurons, which are especially affected in some pathologies, have recently been shown to exhibit HSP mediated by nicotinic acetylcholine receptors (nAChRs). In *Drosophila* central neurons, pharmacological blockade of activity induces a homeostatic response mediated by the *Drosophila* α7 (Dα7) nAChR, which is tuned by a subsequent increase in expression of the voltage-dependent K_V4/Shal channel. Here, we show that an *in vivo* reduction of cholinergic signaling induces HSP mediated by Dα7 nAChRs, and this upregulation of Dα7 itself is sufficient to trigger transcriptional activation, mediated by nuclear factor of activated T cells (NFAT), of the *K_V4/Shal* gene, revealing a receptor-ion channel system coupled for homeostatic tuning in cholinergic neurons.

In Brief

Eadaim et al. show that *in vivo* reduction of cholinergic signaling in *Drosophila* neurons induces synaptic homeostasis mediated by Dα7 nAChRs. This upregulation of Dα7 induces *K_V4/Shal* gene expression mediated by nuclear factor of activated T cells (NFAT), revealing a receptor-ion channel system coupled for homeostatic tuning in cholinergic neurons.

Graphical Abstract

*Correspondence: susan.tsunoda@colostate.edu.

AUTHOR CONTRIBUTIONS

Conceptualization, S.T. and A.E.; Investigation, A.E., E.-T.H., and E.D.J.; Writing- Original Draft, S.T.; Writing- Review and Editing, S.T., A.E., E.-T.H., and E.D.J.; Funding Acquisition, S.T.

DECLARATION OF INTERESTS

The authors declare no competing interests.

SUPPLEMENTAL INFORMATION

Supplemental Information can be found online at https://doi.org/10.1016/j.celrep.2020.108119.

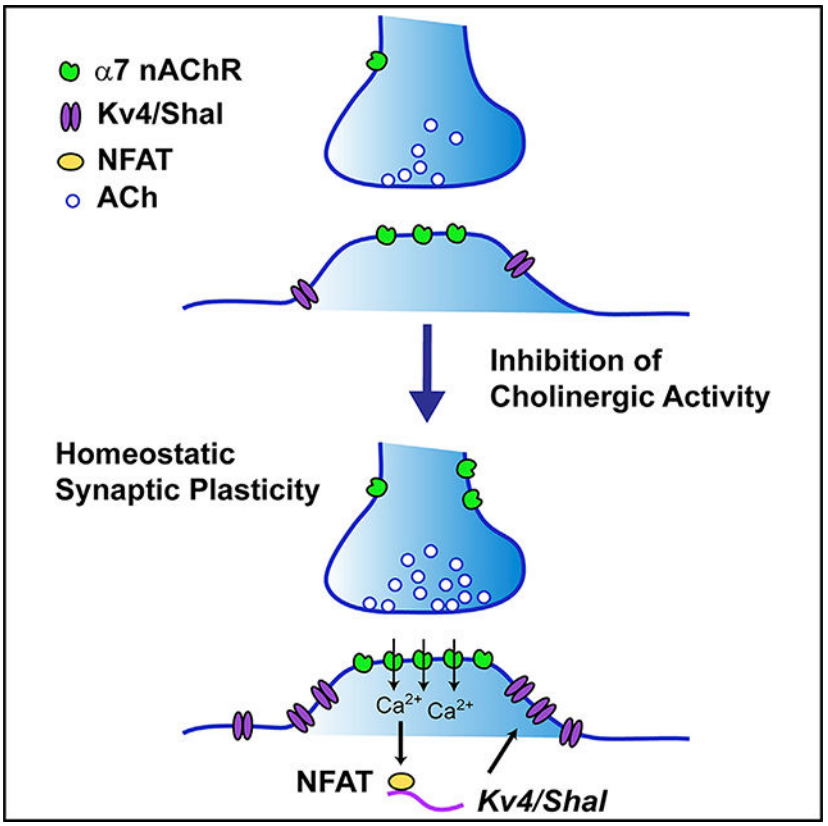

INTRODUCTION

Homeostatic synaptic plasticity (HSP) is thought to function as an adaptive mechanism counterbalancing changes in global neural activity (Davis, 2006; Marder and Goaillard, 2006; Nelson and Turrigiano, 2008; Pozo and Goda, 2010; Turrigiano, 2011, 2008). In general, increasing overall neural activity triggers HSP mechanisms that reduce synaptic strength, while suppressing activity leads to HSP mechanisms that boost synaptic strength. These homeostatic responses have been proposed to come into play during physiological processes, such as learning/memory and development, as well as in response to pathological conditions. Although decades of studies on HSP have focused on glutamatergic synapses, HSP mediated by nicotinic acetylcholine receptors (nAChRs) has also been implicated in numerous pathologies. For example, in patients and models of Alzheimer's disease (AD), nAChRs and cholinergic neurotransmission are increased and decreased at different stages of the disease (Albuquerque et al., 2009; DeKosky et al., 2002; Dineley et al., 2001; Frölich, 2002; Nordberg, 2001; Small and Fodero, 2002), and these changes have been suggested to be homeostatically related (Hahm et al., 2018; Hernandez et al., 2010; Pratt et al., 2011; Small, 2004, 2007). Nicotine dependence has also been shown to involve changes in the expression/function of nAChRs (De Biasi and Dani, 2011; Picciotto et al., 2008), and some studies have suggested that these changes may involve a homeostatic response to the desensitization of nAChRs (Fenster et al., 1999; Ortells and Barrantes, 2010).

Recent studies have verified that nAChRs can indeed mediate HSP (Hahm et al., 2018; Ping and Tsunoda, 2011; Wang et al., 2018). In a previous study, we showed that pharmacological blockade of nAChR activity in primary neurons cultured from *Drosophila* resulted in an increase in synaptic strength that was explained by a selective upregulation of the *Drosophila* α7 (Dα7) nAChR (Ping and Tsunoda, 2011). And, more recently, we showed that early hyperactivity in a *Drosophila* AD model triggers endogenous Dα7-dependent HSP mechanisms that contribute to eventual synaptic depression (Hahm et al., 2018). α7-mediated HSP is intriguing because α7 receptors are among the most abundant and widespread of nAChRs in the mammalian brain and have been implicated in AD, nicotine addiction, nicotine-induced seizure, and schizophrenia (Albuquerque et al., 2009; Steinlein and Bertrand, 2008).

Accurate tuning of HSP, however, is likely to be a critical determinant of whether a homeostatic response is adaptive or maladaptive. For example, if a homeostatic response were to "overshoot" its target activity range, this would result in additional aberrant signaling rather than restoration of effective signaling. We previously showed that Dα7-mediated HSP triggers a tuning mechanism: the upregulation of voltage-gated K_V4/Shal channels, which prevents such an overshoot of the homeostatic response (Ping and Tsunoda, 2011). Whether this occurs when HSP is induced *in vivo* has not been addressed. Little is also known about how inactivity actually leads to the regulation of *K_V4/Shal* expression. Here, we use genetic mutants to reduce activity *in vivo* and investigate the mechanisms underlying inactivity-induced *K_V4/Shal* expression. We show that *K_V4/Shal* expression is responsive to, and dependent on, changing levels of Dα7 nAChRs. We also show that it is indeed *K_V4/Shal* mRNA levels that are dynamic, and this regulation is dependent on the transcriptional activator, nuclear factor of activated T cells (NFAT). In addition, we find that increased expression of Dα7 nAChRs, or the Dα7 regulator NACHO, is sufficient to upregulate K_V4/Shal expression, revealing a receptor-ion channel system, coupled for homeostatic tuning.

RESULTS

Cha^{ts2}-Induced Activity Loss Induces a Homeostatic Response

Previously, we showed that prolonged pharmacological blockade of neural activity in cultured *Drosophila* neurons results in a homeostatic increase in synaptic activity that triggers a subsequent upregulation of K_V4/Shal channel levels, as a mechanism for tuning the homeostatic response (Ping and Tsunoda, 2011). Here, we set out to examine whether we could apply an *in vivo* blockade of activity and detect a similar homeostatic response and upregulation of K_V4/Shal. Since the predominant excitatory neurotransmitter in the *Drosophila* CNS is acetylcholine (ACh), we used temperature-sensitive mutants of the *cholineacetyl transferase* (*ChAT*) gene, referred to as *Cha^{ts}* alleles (Greenspan et al., 1980). *Cha^{ts}* mutations reduce/disable enzyme activity when exposed to elevated temperatures. For example, homozygous *Cha^{ts2}* mutants have been shown to display a ~75% reduction in ChAT activity at 30ºC (Kitamoto et al., 2000; Salvaterra and McCaman, 1985). However, since homozygous *Cha^{ts2}* mutants exhibit significantly reduced levels of ChAT activity even at permissive temperatures (18ºC) (Kitamoto et al., 2000; Salvaterra and McCaman, 1985),

we used heterozygous *Cha*^{ts2}/+ mutants, which exhibit ChAT activity more similar to wild type (WT) when grown at 18ºC. *Cha*^{ts2}/+ heterozygotes raised at 30ºC have been reported to exhibit ~35% less ChAT activity compared to WT (Greenspan et al., 1980).

We first tested if inhibition of ACh synthesis in *Cha*^{ts2}/+ mutants could trigger a homeostatic upregulation of miniature excitatory postsynaptic currents (mEPSCs), a standard assessment of synaptic strength. We grew *Cha*^{ts2}/+ primary cultures for 8 days *in vitro* (DIV) at 18ºC, then shifted cultures to 30ºC for increasing durations of time and recorded mEPSCs at room temperature over the next 60 min. With increasing durations of heat treatment (HT), neurons from *Cha*^{ts2}/+ cultures exhibited mEPSCs that were progressively less frequent, displaying significantly longer interevent times (Figures 1A and 1C; no HT, 750.19 ± 57.42 ms; 2/3 h HT, 1192. ± 76.34 ms; 4/5 h HT, 3364.76 ± 195.26 ms; n = 7–8 cells). The reduction in mEPSC frequency is consistent with a progressive decline in availability of ACh from 2 to 5 h. After 2–3 h of HT, however, we also observed a 34% increase in the amplitude of mEPSCs (Figures 1B and 1C; no HT, 6.12 ± 0.05 pA; 2/3 h HT, 9.26 ± 0.19 pA; 4/5 h HT, 7.0 ± 0.16 pA; n = 7–8 cells), demonstrating a postsynaptic compensatory change. These results show that *Cha*^{ts2}-induced activity reduction induces a physiologically detectable homeostatic response and suggest that HSP mechanisms involve a postsynaptic change.

Since previous studies had shown that pharmacological activity blockade results in a concurrent increase in the Dα7 nAChR (Ping and Tsunoda, 2011), we investigated whether inhibition of cholinergic activity in the *Cha*^{ts2}/+ mutant also resulted in an increase in Dα7 nAChRs. Unfortunately, anti-Dα7 antibodies have proven to be problematic when used for immunoblot analysis. However, since *in vitro* studies suggested that homeostatic changes in Dα7 are translationally regulated (Ping and Tsunoda, 2011), we reasoned that a transgenically expressed EGFP-tagged Dα7 protein would likely represent the changes that the endogenous Dα7 protein undergoes. We used the pan-neuronal *elav-Gal4* transgene to drive expression of *Dα7-EGFP* under control of the upstream activating sequence (*UAS-Dα7-EGFP*). We used flies expressing *Dα7-EGFP* in WT and *Cha*^{ts2}/+ backgrounds (*elav-Gal4>> UAS-Dα7-EGFP/+* and *elav-Gal4>> UAS-Dα7-EGFP/Cha*^{ts2}, respectively). In this way, a similar basal level of Dα7-EGFP is constitutively transcribed in both genotypes. Flies were grown at 18ºC, collected at <24 h after eclosion (AE), and subjected to either no HT or 3 h HT at 30ºC to test if *Cha*^{ts2}-induced inactivity homeostatically enhanced Dα7-EGFP protein levels. We found that levels of Dα7-EGFP were indeed enhanced by ~23% in response to *Cha*^{ts2}-induced activity inhibition, compared to untreated flies; in contrast, similar HT induced no change in Dα7-EGFP levels in the absence of the *Cha*^{ts2} allele (Figure 1D). To examine *Cha*^{ts2}-induced upregulation of Dα7 by another approach, we immunostained whole *Cha*^{ts2}/+ brains after either no HT or HT. We used an anti-Dα7 antibody (kindly provided by Dr. Hugo Bellen) that we were able to validate for immunocytochemistry, although unfortunately not for immunoblot analysis. We found that anti-Dα7 signal, which should represent endogenous Dα7, was indeed also increased in HT *Cha*^{ts2}/+ brains (Figure S1). Altogether, our results suggest that reducing cholinergic activity using the *Cha*^{ts2} allele induces a homeostatic increase in mEPSC amplitude that is mediated by an increase in Dα7 nAChRs, consistent with previous *in vitro* findings (Ping and Tsunoda, 2011).

Dα7 nAChRs Are Localized to Somato-Dendritic and Proximal Axonal Compartments

Although mammalian studies have reported α7 nAChRs both pre- and postsynaptically (Duffy et al., 2009; Fabian-Fine et al., 2001; Jones et al., 2004; Jones and Wonnacott, 2004; Levy and Aoki, 2002; Lubin et al., 1999; Pakkanen et al., 2005), less is known about the subcellular localization of nAChRs in *Drosophila*. Dα7 has been localized to dendrites in multiple neurons in the CNS, including the giant fiber neurons that mediate the escape reflex, Kenyon cells (KCs) intrinsic to the mushroom bodies, and motion-sensitive lobula plate tangential cells (Fayyazuddin et al., 2006; Raghu et al., 2009); it is unclear, however, whether Dα7 is also trafficked to any axonal/presynaptic regions of neurons like mammalian α7 receptors.

We first examined anti-Dα7 immunostaining in the brain, which showed widespread expression, albeit with variable intensity, throughout much of the neuropil (Figure S2). Since neuropil regions contain both axonal projections and dendritic arbors, we used the *UAS/Gal4* system to drive expression of *UAS-Dα7-EGFP* in neuronal sub-populations, in which these subcellular compartments are easily distinguished by their anatomy in the intact brain. Previous studies have also shown that expression of *UAS-Dα7-EGFP* results in localization similar to the anti-Dα7 antibody (Fayyazuddin et al., 2006; Leiss et al., 2009). We used the *GH146-Gal4* and *201Y-Gal4* transgenes to drive expression of *UAS-Dα7-EGFP* and *UAS-DsRed* in projection neurons (PNs) of the antennal lobe (AL) or a subset of KCs, respectively. Young adult brains were dissected, immunostained, and imaged by confocal microscopy. In PNs, Dα7-EGFP signal was found in cell bodies (CBs), in the dendrites of glomeruli in the AL, and in the proximal region of the major inner antennocerebral tract (iACT) of axons and throughout axons of the medial ACT (mACT) (Figures 2A and 2B); DsRed signal was seen in all subcellular compartments of the PNs, as expected (Figures 2A and 2B). A recent study has similarly found Dα7-EGFP localization in the proximal iACT in brains from young flies (Hussain et al., 2018). To reduce overall overexpression of Dα7 and the chance of mis-expression, we also performed these experiments in a $D\alpha7^{P\Delta EY6}$ null mutant background and found a similar localization pattern (Figure S3).

In KCs, Dα7-EGFP signal was also found in CBs, which are clustered in a layer just above the calyx (CX), a neuropil structure into which KCs extend their dendrites, as well as in the CX itself (Figures 2C and 2D). KC axons fasciculate into an anteriorly projecting structure called the peduncle (PED) that then branches into five distinct lobes of the MBs; the *201Y-Gal4* transgene drives expression in KCs that extend axons into the α/β and γ lobes. We found Dα7-EGFP signal clearly in the PED (Figures 2C and 2D) but less prominently and perhaps absent from more distal axonal regions that extend into in the mushroom body (MB) lobes (data not shown); a similar localization pattern was also observed in a $D\alpha7^{P\Delta EY6}$ null mutant background (Figure S3).

Altogether, we suggest that Dα7 is localized to somato-dendritic compartments, as well as proximal regions of axonal tracts. Interestingly, when $Cha^{ts2}/+$ mutants were subjected to longer HTs (e.g., 6–7 h), not only were mEPSC amplitudes enhanced, but mEPSC interevent times were also significantly decreased (Figure S4). These results suggest that there may be a later stage of HSP mediated on the presynaptic side of synapses, perhaps involving these axonally localized Dα7 nAChRs.

In Vivo Activity Blockade Induces an Increase in K_V4/Shal Channel Protein That Is Dependent on Dα7

To test if *in vivo* activity inhibition using the *Cha^{ts2}* allele also induces an upregulation of K_V4/Shal channels, newly eclosed *Cha^{ts2}*/+ and WT flies were collected and subjected to HT at 30ºC. We tested different durations of HT, followed by a 3-h recovery period at 18ºC. We found that *Cha^{ts2}/+* flies displayed a ~27% increase in K_V4 protein with a 3- or 6-h HT (Figure 3A); we refer to the 3 or 6 h of HT, followed by 3 h of recovery, as 3/3 or 6/3-protocols, respectively. Similarly treated WT flies showed no change in relative K_V4/Shal protein levels (Figure 3B). Because *in vitro* studies had shown that the upregulation of K_V4/Shal was not apparent immediately following cholinergic blockade (3/0-protocol) but required recovery of synaptic transmission, we subjected *Cha^{ts2}/+* flies to HT for 3 h with different durations of recovery. Indeed, we found that no increase in K_V4/Shal was observed immediately following activity inhibition and required a 3-h recovery period (Figure 3C). For further confirmation that HT of *Cha^{ts}* was a reliable method of inducing HSP, we tested another *Cha^{ts}* allele, *Cha^{ts3}* (Kitamoto et al., 2000). Heterozygous *Cha^{ts3}/+* flies subjected to the 3/3-protocol also exhibited ~29% increase in K_V4/Shal protein (Figure 3D).

We also inhibited cholinergic activity by another approach, using a transgenic line that expresses tetanus toxin light chain (TnT), which cleaves n-synaptobrevin and has been shown to completely block evoked neurotransmitter release and reduce spontaneous release by 50%–75% (Deitcher et al., 1998; Sweeney et al., 1995). We used a *Chat-Gal4* line, which drives expression of Gal4 in ChAT-expressing neurons, to induce expression of *UAS-TnT.* To induce expression transiently, we included expression of the temperature-sensitive Gal80 protein (Gal80^{ts}) to negatively regulate the function of Gal4. At 18ºC, Gal80^{ts} inhibits Gal4; at 30ºC, Gal80^{ts} is no longer functional, and Gal4 promotes transcription of the *UAS-TnT* transgene in cholinergic neurons. We raised *Chat-Gal4/tub-Gal80^{ts}>>UAS-TnT* and WT lines at 18ºC to allow them to develop normally, without expression of *UAS-TnT*, then AE, young adult flies were subjected to HT at 30ºC for 3 or 6 h. After HT, we allowed flies to recover at 18ºC for 3 h. Fly heads were analyzed by immunoblot analysis for steady-state levels of K_V4/Shal normalized to a loading control protein. We found that levels of K_V4/Shal were increased by 42% after a 6/3-protocol (Figure 3E).

We next tested if the upregulation of K_V4/Shal induced by *in vivo* activity blockade requires the Dα7 nAChR. 0/0- and 3/3-protocols were applied to *Cha^{ts2}*/+ flies in a *Dα7^{PΔEY6}* null mutant background (*Dα7^{PΔEY6};;Cha^{ts2}*/+). We found that in the absence of Dα7 nAChRs, *Cha^{ts2}*-induced upregulation of K_V4/Shal was indeed inhibited (Figure 3F), suggesting a requirement for the Dα7 nAChR. Together, our results suggest that *in vivo* inhibition of cholinergic activity induces a homeostatic upregulation of Dα7 nAChRs that is required for the subsequent increase in K_V4/Shal protein.

Activity Inhibition Induces Upregulation of K_V4/Shal Current

We then tested whether *Cha^{ts2}*-mediated activity inhibition would also induce a detectable increase in K_V4/Shal current in neurons. Primary cultures were grown at 18ºC for 8 DIV, then subjected to HT at 30ºC for 6 h followed by 2–3 h of recovery at 18ºC. Previous studies have identified K_V4/Shal currents in these neurons as the predominant A-type K^+ current

present, one that can easily be isolated from the delayed rectifier (DR) currents encoded by K_v2 (*Shab*) and K_v3 (*Shaw*) (Tsunoda and Salkoff, 1995a, 1995b). Because of the hyperpolarized closed-state inactivation properties of K_V4/Shal channels, a 500-ms prepulse at −45 mV specifically inactivates K_V4/Shal channels in these neurons, and the K_V4/Shal current can be isolated by subtracting the DR component from the whole-cell current (Ping and Tsunoda, 2011; Ping et al., 2011a; Tsunoda and Salkoff, 1995a, 1995b). Indeed, K_V4/Shal current density in HT $Cha^{ts2}/+$ neurons was 67% and 88% greater than in non-HT $Cha^{ts2}/+$ neurons or in HT background control neurons, respectively (Figure 4); HT alone did not induce a change in K_V4/Shal current density in genetic background control neurons (Figure 4).

In Vivo Activity Blockade Also Induces a Dα7-Dependent Increase in $K_V4/Shal$ mRNA

Although inactivity-induced upregulation of Kv4/Shal protein was previously shown to be blocked by transcriptional inhibitors (Ping and Tsunoda, 2011), it has been unclear whether this was due to a transcriptional block of $K_V4/Shal$ itself since mRNA levels of $K_V4/Shal$ could not be examined in that preparation. Our *in vivo* Cha^{ts2} and *ChAT-Gal4/tub-GAL80^{ts}>>UAS-TnT* models, however, allowed for sufficient mRNA to be isolated for quantitative reverse transcriptase polymerase chain reactions (qRT-PCR). We examined if mRNA levels of $K_V4/Shal$ are indeed elevated following activity blockade. To this end, we validated universal probes with corresponding PCR primers for efficient amplification and optimized RNA preparation, RT reactions, and cDNA dilution factors for reliable qRT-PCR (see Method Details). For every experimental genotype and genetic background tested, the stability of each of the reference genes, *ribosomal protein S20* (*RpS20*) and *eukaryotic initiation factor 1A* (*eIF1A*), was validated before use (see Method Details).

We tested both the *Chat-Gal4/tub-Gal80^{ts}>>UAS-TnT* and $Cha^{ts2}/+$ line immediately after inhibiting activity with a 6-h or 3-h HT at 30ºC, respectively, each of which leads to an upregulation of K_V4/Shal protein that is detectable after a subsequent 3 h of recovery (Figures 3A and 3E). We quantified $K_V4/Shal$ mRNA levels relative to reference gene expression without HT (0/0) and after 6 or 3 h HT (6/0 or 3/0, respectively). In WT, $K_V4/Shal$ mRNA levels showed no change with HT (Figures 5A and 5B, left). In contrast, when HT was applied to *Chat-Gal4;tub-Gal80^{ts}>>UAS-TnT* or $Cha^{ts2}/+$ lines, $K_V4/Shal$ mRNA levels were significantly elevated by 27% and 23% compared to untreated controls, respectively (Figures 5A and 5B, right). Interestingly, the rise in $K_V4/Shal$ mRNA was rather short-lived when examined in Cha^{ts2} flies, returning to baseline levels after 3 h of recovery at 18ºC (3/3-protocol; Figure 5B, right), suggesting a transient and dynamic regulation of $K_V4/Shal$ mRNA.

We next tested whether the inactivity-induced upregulation of $K_V4/Shal$ mRNA is dependent on Dα7 nAChRs, as was the increase in K_V4/Shal protein (see Figure 3F). We examined relative $K_V4/Shal$ mRNA levels in $D\alpha7^{P\Delta EY6}$;;Cha^{ts2}/+ flies. We found that the 3/0-protocol that induced an increase in $K_V4/Shal$ mRNA in $Cha^{ts2}/+$ mutants resulted in no significant increase in $K_V4/Shal$ mRNA in the $D\alpha7^{P\Delta EY6}$ null background (Figure 5C, right); as an additional control, we tested $D\alpha7^{P\Delta EY6}$ null mutants alone and found no change in $K_V4/Shal$ mRNA levels with HT (Figure 5C, left). Together, our results show that cholinergic activity

blockade/inhibition induces an increase in *K_V4/Shal* mRNA, and this upregulation in *K_V4/Shal* mRNA is dependent on Dα7 nAChRs.

Increased Expression of Dα7 is Sufficient to Upregulate K_V4/Shal Channel Protein and mRNA

We next tested if upregulation of Dα7-EGFP alone is sufficient to induce an increase in K_V4/Shal channel protein and mRNA. To transiently induce expression of *UAS-Dα7-EGFP*, we generated *elav-Gal4;tub-Gal80^{ts}>>UAS-Dα7-EGFP/+* lines. We raised *elav-Gal4;tub-Gal80^{ts}>>UAS-Dα7-EGFP/+* and background control lines at 18ºC to allow them to develop normally, without overexpression of Dα7-EGFP, and then AE, young adult flies were subjected to HT at 30ºC for 4 days to induce expression of Dα7-EGFP (Figure 6A). We then tested whether this post-eclosion overexpression of Dα7-EGFP induced an increase in steady-state level of K_V4/Shal protein. Indeed, we found that induced expression of Dα7-EGFP resulted in K_V4/Shal protein levels that were elevated by ~14% (Figure 6A, left). Similar upregulation of K_V4/Shal was also observed when we used a *Dα7-Gal4* driver (Figure S5).

To further test the Dα7-K_V4/Shal relationship, we set out to increase the expression of endogenous *Dα7* and test for effects on K_V4/Shal. Recent studies have identified NACHO as a transmembrane endoplasmic reticulum resident protein that promotes biogenesis and surface expression of nAChRs (Matta et al., 2017) and, in particular, α7 nAChRs (Gu et al., 2016). Thus, we aimed to overexpress the *Drosophila* ortholog of NACHO in neurons, as a way of increasing the expression/trafficking of endogenous Dα7 nAChRs, and then test if this results in a consequent increase in K_V4/Shal expression. We used an *UAS-NACHO-3xHA* transgenic line in combination with *elav-Gal4* and *tub-Gal80^{ts}* transgenes to conditionally overexpress *UAS-NACHO-3xHA* in the nervous system of adult flies. The 3xHA epitope tag was used to confirm expression of NACHO-3xHA. We raised *elav-Gal4;tub-Gal80^{ts}>>UAS-NACHO-3xHA* and background control lines at 18ºC, and then AE, flies were subjected to HT at 30ºC. Interestingly, *elav-Gal4;tub-Gal80^{ts}>>UAS-NACHO-3xHA* flies, which were homozygous for the *UAS-NACHO-3xHA* insertion, were only viable for 12–15 h at 30ºC. As such, we assayed K_V4/Shal protein at 12 h and found that K_V4/Shal protein levels were indeed elevated in HT *elav-Gal4;tub-Gal80^{ts}>>UAS-NACHO-3xHA* flies by ~33%, while no change in K_V4/Shal was observed in similarly treated background control lines (Figure 6B).

Interestingly, K_V4/Shal protein levels were increased by ~33% with NACHO overexpression but were increased by only ~14% with Dα7-EGFP overexpression. One possibility is that endogenous NACHO is limiting when Dα7-EGFP is overexpressed, preventing maximal Dα7/Dα7-EGFP surface expression and thereby more limited upregulation of K_V4/Shal. To address this, we conditionally overexpressed both *UAS-NACHO-3xHA* and *UAS-Dα7-EGFP*, using the *elav-Gal4;tub-Gal80^{ts}* driver line. To allow for more balanced expression of NACHO-3xHA and Dα7-EGFP, experimental and background control lines used were heterozygous for each insertion. Both lines were raised at 18ºC during development, and then AE, flies were subjected to HT at 30ºC. With co-expression of *UAS-NACHO-3xHA/UAS-Dα7-EGFP*, flies lived longer than those overexpressing two copies of *UAS-*

NACHO-3x-HA alone, allowing us to apply HT for days. We then examined how co-overexpression of NACHO-3xHA and Dα7-EGFP affected K_V4/Shal protein levels. We found that Kv4/Shal protein levels more than tripled (Figure 6C). To confirm that overexpression of the NACHO-3xHA fusion protein does indeed result in increased Dα7/Dα7-EGFP levels, we compared transgenic lines expressing Dα7-EGFP with and without NACHO-3xHA expression. We found that, indeed, Dα7-EGFP levels were elevated by ~45% when NACHO-3x-HA was expressed (Figure 6D). Interestingly, we also found that RNAi knockdown of *NACHO* prevented any Cha^{ts2}-induced increase in K_V4/Shal (Figure 6E), suggesting that NACHO is required for the inactivity-induced upregulation of K_V4/Shal.

We next tested if induced expression of Dα7-EGFP and/or NACHO results in an elevation in $K_V4/Shal$ mRNA. We used the *elav-Gal4* driver in combination with the temperature-sensitive Gal80 protein, as performed when examining K_V4/Shal protein expression. For each genotype, we assayed for $K_V4/Shal$ mRNA levels at times prior to detected elevations in K_V4/Shal protein (see Figures 3, 5, and 6). Indeed, $K_V4/Shal$ mRNA levels were enhanced by Dα7-EGFP or NACHO overexpression (Figures 6A and 6B, right) and similar to induced K_V4/Shal protein levels, even more so by overexpression of Dα7-EGFP and NACHO (Figure 6C, right). Together, our results suggest that an increase in Dα7-EGFP alone is sufficient to trigger an upregulation of $K_V4/Shal$ mRNA and protein expression.

Cha^{ts2}-Induced Inactivity, or Overexpression of Dα7, Activates the NFAT-Based CaLexA Reporter

With mounting evidence that $K_V4/Shal$ is dynamically and transcriptionally regulated downstream of changing neural activity and Dα7 nAChR levels, we set out to identify transcriptional regulators involved. Previously, we demonstrated that the inactivity-induced increase in K_V4/Shal was dependent on intracellular Ca^{2+}, likely enhanced by the increased number of Ca^{2+}-permeable Dα7 nAChRs (Ping and Tsunoda, 2011). We considered Ca^{2+}-dependent transcriptional regulators, including NFATs, which are activated by the Ca^{2+}-dependent protein phosphatase 2b, calcineurin (CaN). CaN has been shown to trigger translocation of mammalian NFATs into the nucleus, where they lead to increases or decreases in transcription (Macián et al., 2001; Mognol et al., 2016; Rao et al., 1997). To test if NFAT might be a Ca^{2+}-dependent transcriptional regulator involved in the inactivity-induced upregulation of $K_V4/Shal$, we first examined if inactivity induced with the Cha^{ts2} allele would activate an *in vivo* NFAT-based reporter system, the Ca^{2+}-dependent nuclear import of LexA (CaLexA) system (Masuyama et al., 2012). In the CaLexA system, a transgene containing the regulatory domain of human NFATc1 is fused to the mutant bacterial DNA-binding protein mLexA and the VP16 activation domain, *UAS-mLexA-VP16-NFAT*. When the mLexA-VP16-NFAT protein is expressed, it is cytoplasmic, and if the NFAT regulatory domain is activated, the fusion protein translocates to the nucleus, where it promotes transcription from a *LexAop* sequence upstream of a reporter gene. This modified human NFAT has been shown to successfully translocate to the nucleus and drive expression of *LexAop-CD2/8-GFP* in the fly CNS and has been used as a Ca^{2+} reporter (Masuyama et al., 2012).

We used *elav-Gal4* to drive neuronal expression of *UAS-mLexA-VP16-NFAT*, in a $Cha^{ts2}/+$ mutant background, which also contained two reporter insertions, *LexAop-CD8-GFP* and *LexAop-CD2-GFP*. These flies were subjected to 0/0 and 3/0 HT (30ºC) protocols. We then tested for CD8/CD2-GFP expression by immunoblot analysis, as an indicator for CaLexA activation. Indeed, we found that CD8/CD2-GFP expression was increased by ~49% with the 3/0-protocol, compared with age-matched flies not subjected to HT (0/0) (Figure 7A, left), and levels of CD8/CD2-GFP continue to rise with additional recovery time after HT (Figure S6). In contrast, *elav-Gal4>>UAS-mLexA-VP16-NFAT/LexAop-CD8-GFP;LexAop-CD2-GFP/+* lines, without the Cha^{ts2} allele, showed no increase in CD2/8-GFP with the same HT. These results suggest that inactivity induced by Cha^{ts2} does indeed activate an NFAT-based reporter system *in vivo*.

We additionally tested whether overexpression of Dα7-EGFP alone was sufficient to activate the CaLexA reporter. We raised *elav-Gal4;tub-Gal80^{ts}>>UAS-Dα7-EGFP/UAS-mLexA-VP16-NFAT,LexAop-CD8-GFP;LexAop-CD2-GFP/+* flies at 18ºC to allow for normal development, and then AE, young adult flies were subjected to HT at 30ºC to induce expression of Dα7-EGFP. Because HT on the order of days was required to observe sufficient overexpression of Dα7-EGFP using the *elav-Gal4;tub-Gal80^{ts}*-inducible driver to induce K_V4/Shal expression (Figure 6A), we expected that activation of the CaLexA reporter would require at least 24 h HT to induce sufficient overexpression of Dα7-EGFP. We found that CD8/CD2-GFP reporter expression more than doubled after 24 h of heat-induced Dα7-EGFP expression compared to HT of the background control line, *elav-Gal4;tub-Gal80^{ts}>>UAS-mLexA-VP16-NFAT,LexAop-CD8-GFP/+;LexAop-CD2-GFP/+* (Figure 7A, right). Our results demonstrate that inactivity, which homeostatically upregulates Dα7, or even direct overexpression of Dα7, is sufficient to activate an NFAT-based reporter system and possibly endogenous NFAT itself.

NFAT Is Required for Inactivity-Induced Upregulation of *K_V4/Shal*

We next investigated whether NFAT might be involved in the regulation of *K_V4/Shal* expression. In *Drosophila*, there is only a single *NFAT* gene (Keyser et al., 2007) that is 53%–64% similar to mammalian NFATs (Freeman et al., 2011). *Drosophila NFAT* has two predicted splice forms, *−A* and *−B*, generated from two different promoter sites (Keyser et al., 2007). We obtained mutants that have been generated and verified to eliminate both *NFAT* splice forms ($NFAT^{\Delta AB}$), *NFAT-A* only ($NFAT^{\Delta A}$), or *NFAT-B* only ($NFAT^{\Delta B}$) (Freeman et al., 2011; Keyser et al., 2007). First, we tested flies that were null mutants for either or both *NFAT-A* and/or *NFAT-B* and compared them to WT controls. We found no significant difference in steady-state K_V4/Shal protein or mRNA levels (Figure 7B), suggesting that NFAT does not regulate basal levels of *K_V4/Shal* expression.

Next, we tested if NFAT is required for the inactivity-induced upregulation of *K_V4/Shal*. We crossed *NFAT* mutant alleles into the $Cha^{ts2}/+$ mutant background and assayed whether inhibition of activity could still induce an upregulation of K_V4/Shal protein in these flies. We subjected mutant combinations of Cha^{ts2} with $NFAT^{\Delta A}$, $NFAT^{\Delta B}$, or $NFAT^{\Delta AB}$, as well as background control lines, to the 0/0- and 3/3-protocols that upregulate K_V4/Shal expression in $Cha^{ts2}/+$ mutants. We found that Cha^{ts2}-induced inactivity was unable to elicit an increase

in K_V4/Shal protein in the absence of *NFAT-A* and/or *NFAT-B* (Figures 7C–7E, left); *NFAT* mutant alleles alone also showed no difference in K_V4/Shal levels with HT.

We then tested these same genotypes for inactivity-induced upregulation of *K_V4/Shal* mRNA. We subjected flies to the 0/0- and 3/0-protocols in which an upregulation in *K_V4/Shal* mRNA is detected following inactivity. Similar to K_V4/Shal protein analyses, we found that a loss of *NFAT-A* and/or *NFAT-B* blocked the upregulation of *K_V4/Shal* mRNA (Figures 7C–7E, right); HT of *NFAT* alleles alone also had no effect on *K_V4/Shal* mRNA levels. Altogether, our results suggest that while NFAT does not affect basal levels of *K_V4/Shal* mRNA or protein, NFAT is required for the transient upregulation of K_V4/Shal *mRNA* and protein induced by cholinergic activity blockade.

DISCUSSION

While HSP has been widely studied at glutamatergic synapses, less is known about these mechanisms at cholinergic synapses. Proper tuning of HSP at any synapse is critical for neuroprotection since over-/under-compensation is likely to be maladaptive. Here, we inhibit activity that evokes a homeostatic increase in mEPSC amplitude that correlates with an increase in Dα7 nAChR protein as well as a subsequent increase in K_V4/Shal channel expression that is dependent on Dα7 receptors. We show that regulation of *K_V4/Shal* is at the mRNA level and is dependent on the transcriptional regulator, NFAT. We also show that upregulation of K_V4/Shal can be induced by an increase in Dα7 nAChRs alone, demonstrated by overexpressing Dα7-EGFP and/or the recently identified α7 chaperone protein, NACHO, and suggesting that there is a homeostatic Dα7-K_V4/Shal regulatory pathway that has evolved to prevent over-excitation whenever there is an over-production of Dα7 nAChRs.

α7 nAChRs are known to be highly abundant in the mammalian brain, and their Ca^{2+}-permeability makes them ideal candidates for mediating different forms of plasticity. As such, preventing over-activity of these receptors is likely to be important, and the “coupling” of K_V4/Shal expression to levels of Dα7 receptors is a mechanism that would act as a protective “brake.” Because K_V4/Shal channels have been shown to open at subthreshold potentials and regulate mEPSCs as well as the time to first action potential firing (Ping and Tsunoda, 2011; Ping et al., 2011a), they make good modulators for tuning subthreshold membrane potentials. Indeed, regulation of K_V4/Shal channels has been shown to be involved in other forms of synaptic plasticity, including long-term-potentiation (LTP) (Chen et al., 2006; Jung and Hoffman, 2009; Kim et al., 2007). Future studies will need to investigate if newly upregulated K_V4/Shal channels are trafficked to specific synapses, perhaps to sites where Dα7 nAChRs have been especially enhanced, for local modulation of membrane potential.

Our study also shows that *in vivo* induction of NACHO-3xHA results in an upregulation of total Dα7-EGFP protein and K_V4 channel protein. With two copies of *UAS-NACHO-3xHA*, and likely stronger induction of NACHO-3xHA, the increase in K_V4 occurs within 12 h. It is unclear whether, in this rather short amount of time, this is due to an increased steady-state level of Dα7 protein and/or facilitated Dα7 release from the endoplasmic reticulum (ER)

that results in increased surface expression. Future studies will need additional approaches to study how NACHO functions in the trafficking and/or stabilization of Dα7 nAChRs.

Finally, we show that the Ca^{2+}/CaN-dependent transcriptional regulator, NFAT, is involved in the inactivity/Dα7-induced increase in *K_V4/Shal* expression. Other studies have also implicated NFATs in the regulation of ion channels, especially in the cardiovascular system. For example, in arterial smooth muscle, the vasoactive peptide, angiotensin II, induces an increase in Ca^{2+} through L-type Ca^{2+} channels that subsequently leads to a CaN-NFATc3-dependent downregulation of *$K_V2.1$* channel expression (Amberg et al., 2004). During hypertension, NFATc3 has also been implicated in the downregulation of the *β1* subunit of large/big conductance Ca^{2+}-activated K^+ (BK) channels (Nieves-Cintrón et al., 2007). In cardiomyocytes, NFATc3 is reported to decrease *$K_V4.2$* expression in response to myocardial infarction (Rossow et al., 2004) and to increase *$K_V4.2$* expression during cardiac hypertrophy (Gong et al., 2006). NFATc3 has also been reported to contribute to the gradient of *K_V4* expression across the mouse left ventricular free wall (Rossow et al., 2006). In neurons of the rat superior cervical ganglion (SCG), increases in activity were shown to induce activation of NFATc1/c2, which leads to an increase in *K_V7* channel expression (Zhang and Shapiro, 2012). In cerebellum granule neurons, Ca^{2+}/CaN-NFATc4 signaling underlies the upregulation of *$K_V4.2$* expression in response to the neurotrophin, neuritin (Yao et al., 2016). In *Drosophila*, overexpression of one splice form of the single *NFAT* gene has been shown to result in the suppression of excitability in motor neurons (Freeman et al., 2011), although the ion channels involved have not been identified. We used the same overexpression line but found no significant increase in K_V4/Shal. It is possible that activated NFAT is required to induce HSP and upregulation of K_V4/Shal, rather than solely an increase in basal levels of NFAT. Future studies will also need to address whether activated NFAT acts directly on the *K_V4* locus.

Uncovering how HSP mechanisms are tuned to accurately protect neurons from over-/under-activity is critically important to understanding how an adaptive HSP response can become maladaptive. For example, HSP has been reported to be impaired or maladaptive in mouse and *Drosophila* AD models (Gilbert et al., 2016; Hahm et al., 2018; Jang and Chung, 2016). Interestingly, K_V4/Shal channels examined in this study, which tune HSP in cholinergic neurons, have been shown to be especially affected in various models of AD, and genetic restoration of K_V4/Shal channels ameliorates downstream pathologies (Hall et al., 2015; Ping et al., 2015; Scala et al., 2015), supporting the idea that tuning HSP by K_V4/Shal channels is critically important. With a better understanding of how HSP is accurately tuned, these molecules and mechanisms may be identified as potential targets for treatment when HSP becomes maladaptive.

STAR★METHODS

RESOURCE AVAILABILITY

Lead Contact—Further information and requests should be directed to, and will be fulfilled by the Lead Contact, Susan Tsunoda (susan.tsunoda@colostate.edu).

Materials Availability—This study did not generate new unique reagents.

Data and Code Availability—This study did not generate any unique datasets or code.

EXPERIMENTAL MODEL AND SUBJECT DETAILS

***Drosophila* Stocks—** w^{1118} or genetic background strains were used as control lines in this study. We used previously generated mutant and transgenic lines: *UAS-TnT* (Deitcher et al., 1998; Sweeney et al., 1995); Cha^{ts2} and Cha^{ts3} alleles (Salvaterra and McCaman, 1985); *UAS-Dα7-EGFP* (Leiss et al., 2009) and $Dα7^{PΔEY6}$ (Fayyazuddin et al., 2006); *UAS-NACHO-3xHA* (Bischof et al., 2013); *UAS-mLexA-VP16-NFAT, LexAop-CD8-GFP,* and *LexAop-CD2-GFP* transgenes (Masuyama et al., 2012); $NFAT^{ΔAB}$, $NFAT^{ΔA}$, and $NFAT^{ΔB}$ alleles (Keyser et al., 2007); *elav-GAL4* (*elav-GAL4*^{c155}) and *tub-GAL80*^{ts} (Bloomington *Drosophila* Stock Center, Indiana University); *201Y-GAL4* (O'Dell et al., 1995; Yang et al., 1995); *GH146-GAL4* (Stocker et al., 1997); *UAS-RNAi-NACHO* (VDRC, Vienna, Austria), *Dα7-GAL4* (Fayyazuddin et al., 2006). All *Drosophila* stocks were raised at 18–25ºC as specified in text, on standard fly food medium.

METHOD DETAILS

Reverse Transcription-Quantitative Polymerase Chain Reaction (qRT-PCR)

RNA isoloation, Reverse Transcription, and qPCR: Total RNA was extracted from 10 fly heads using TRIzol reagent, treated with DNase I (Thermo Scientific) to remove potential genomic DNA contamination. The integrity of the representative RNA samples was assessed using gel electrophoresis. Total RNA concentration was measured in duplicate using NanoDrop Lite Spectrophotometer (Thermo Scientific) and the purity of the samples was estimated by the OD ratios (A260/A280, ranging within 1.9–2.0). cDNA was synthesized from 700 ng of DNA-free total RNA in a 20 μl reaction volume using SuperScript II RT (Invitrogen) and Oligo (dT) as reverse transcription primers. cDNA samples were diluted 1:5 for qPCR reactions. Gene-specific transcription levels were determined in a 20-μl reaction volume in triplicate using a probe from the Universal Probe Library (UPL) and Light Cycler® 480 (Roche) following the manufacturer's instructions; under the following conditions: incubation at 95ºC for 10 min, followed by 45 cycles of 95ºC for 10 s and 60ºC for 30 s and 72ºC for 1 s.

Primer design and verification—Common sequence from multiple mRNA transcript variants (predicted in Fly Base) were used for PCR primer design. Probe finder version 2.35 and intron spanning assay (Roche) were used to find a proper probe and design primers; Primer3 software was used with the following settings: melting temperatures between 59ºC and 61ºC, GC content between 40 and 60% and amplicon length limited to 60–200 base pairs. The maximum self-complementarity of the primers was set at 8 and the maximum 3′ complementarity at 3. The PCR primer sets specificity were verified by Primer-Blast (http://www.ncbi.nlm.nih.gov/tools/primer-blast/) using the *Drosophila* transciptome. Probe 66 was used for *Kv4/Shal* primers (*Left*, GCTAACGAAAGGAGGAACG; *Right*, TGAACTTATTGCTGTCATTTTGC) and *RPS20* primers (*Left,* CGACCAGGGAAATTGCTAAA; *Right*, CGACATGGGGCTTCTCAATA); Probe 147 was used for *eIF1A* primers (*Left*, TCG TCT GGA GGC AAT GTG; *Right*, GCC CTG GTT AAT CCA CAC C). Real-time products were extracted for sequencing and PCR efficiency

was calculated from 10-fold serial dilutions of cDNA samples; only PCR efficiencies of 1.9–2.0 were accepted. Similarity in GOI and Reference gene amplification efficiencies were verified, which allowed us to use $2^{-\Delta\Delta ct}$ method for data analysis. Ribosomal Protein S 20 (RpS20) and Eukaryotic Initiation Factor 1 A (eIF1A) were selected as reference genes based on their stability across experimental conditions.

Data Analysis—After completing each real-time PCR run, outlier C_t values among each triplicate were identified and excluded manually using the Q-test. Individual ΔΔCt values were calculated as the difference between ΔCt (Experimental or Control) and the average ΔCt (Control) value; ΔCt is the difference between averaged triplicate Ct values of the GOI and triplicate Ct values of the reference gene. ΔΔCt values were used to calculate $2^{-\Delta\Delta ct}$ values, which represent relative fold-changes of the GOI in the experimental group relative to the GOI in the control group.

Digital Drop PCR—RNA isolation, RT reactions, primers and probes for K_v4/Shal and reference gene amplification are as described for RT-qPCR. To generate droplets, the 20ul PCR reaction mix and 60ul droplet generation oil were added to wells in a DG8 Cartridge for the QX200 Droplet Generator (Bio-Rad Laboraties). After automated droplet generation, droplets were transferred to a 96-well plate. The plate was sealed with foil using the PX1 PCR Plate Sealer (Bio-Rad Laboratories), and PCR amplification was performed (C1000 Touch Thermal Cycler, Bio-Rad Laboratories). The following thermal cycling protocol was used: 95ºC for 10 minutes (one cycle), 94ºC for 30 s (40 Cycles) and then 60ºC for 1 minute (40 cycles), 98ºC for 1 minutes (one cycle), hold at 4ºC. The ramp rate was set at 2ºC/s, the sample volume at 40 mL, and the heated lid at 105ºC. After PCR amplification, plate was read in the QX200 Droplet Reader (Bio-Rad Laboratories). Absolute template expression in copies per microliter were quantified using QuantaSoft software (Bio-Rad Laboratories); number of K_v4/Shal copies/ul were normalized to the number of RpS20 copies/ul from the same RNA sample.

Immunoblot Analysis—For each sample, five adult *Drosophila* heads were sonicated in SDS sample buffer (50 mM Tris–HCl, ph 6.8, 10% SDS, glycerol, Dithiothreitol (DTT), bromophenol blue); N refers to the number of samples tested. Proteins were separated on a 10% acrylamide gel. Nitrocellulose blots were probed with primary antibodies overnight at room temperature: anti-Kv4/Shal 1:100, anti-actin 1:10000 (EMD Millipore), anti-GFP 1:10000 (Torrey Pines Biolabs); anti-HA 1:500 (Covance Research Products), and anti-syntaxin 1:50 (Developmental Hybridoma Studies Bank). Anti-K_v4/Shal antibodies were generated as previously described (Diao et al., 2010, 2009). Blots were incubated with peroxidase-conjugated secondary antibodies (1:1000; Jackson ImmunoResearch Laboratories) for one hour at room temperature, developed using Supersignal Signal™ West Pico PLUS (Thermo Scientific). K_v4/Shal, GFP, and HA signal densities were normalized to densities from loading control signals from the same lane.

Electrophysiological Recordings—For neuronal cultures, single embryos aged 5–6 hours (at room temperature) were dissociated in drop cultures of 20 μL culture medium, as previously described (Ping and Tsunoda, 2011; Tsunoda and Salkoff, 1995a, 1995b).

Cultures were grown for up to 2 weeks in a humidified chamber at room temperature. Whole-cell recordings were performed in perforated patch-clamp configuration by adding 400 – 800 μg/ml Amphotericin-B (Sigma-Aldrich) in the pipette, as described previously (Ping and Tsunoda, 2011; Ping et al., 2011a). We used external solution (in mM): NaCl, 140; KCl, 2; HEPES, 5; $CaCl_2$, 1.5; $MgCl_2$, 6; pH 7.2. For mEPSC recordings, TTX (1 μM) was added to the external solution to block voltage-dependent Na^+ channels. Electrodes were filled with internal solution (in mM): K-gluconate, 120; KCl, 20; HEPEs, 10; EGTA, 1.1; $MgCl_2$, 2; $CaCl_2$, 0.1; ATP-Mg, 4; pH 7.2. All recordings were performed at room temperature. Gigaohm seals were obtained for whole-cell recordings. Data was acquired and analyzed using an Axopatch 200B amplifier, Axon Digidata 1550 and pClamp 10 software (Molecular Devices Corp.). Recordings were digitized at 5 kHz and filtered at 2 kHz, using a lowpass Bessel filter.

Immunostaining, Confocal Microscopy, and Image Processing—Fixation and staining of 1–3 day old adult fly brains dissected in 1X PBS on ice was performed as previously described (Daubert and Condron, 2007). Primary antibodies used were chicken anti-GFP (1:2000, Aves Labs), rabbit anti-RFP (1:2000, Rockland Immunochemicals Inc.), and rat anti-Dα7 (1:2000, a gift from Dr. Hugo Bellen; Fayyazuddin et al., 2006). Alexa Fluorophores, anti-chicken 488, anti-rabbit 568, and anti-rat 488 and 568 from Invitrogen were used at a 1:2000 dilution. Fluorescent imaging was performed with Zeiss LSM 710 or LSM 800 confocal microscope, and images were analyzed in ImageJ. Images of Dα7-GFP expression were processed using the “Despeckle” noise filter in ImageJ before maximum intensity Z-projections were generated.

Quantification of Dα7 labeling—< 24 hour old adult male Cha^{ts2}/+ flies were either kept at 18ºC for 9 hours (0/0) or heat-shocked at 30ºC for 6 hours followed by 3 hours recovery at 18ºC (6/3). Brains from both groups were then dissected and fixed onto the same glass coverslip in 4% PFA for 7 minutes to ensure identical treatment. This short fixation time was previously found to generate the best labeling with the rat anti-Dα7 antibody (Fayyazuddin et al., 2006; Raghu et al., 2009). Subsequent immunohistochemical steps were as described. Brains from each independent experiment were imaged on the same day with the same settings using a Zeiss LSM 710 confocal microscope.

QUANTIFICATION AND STATISTICAL ANALYSIS

All experiments were conducted multiple times with multiple samples per condition, as indicated. Q-tests were run to identify outliers, and an upaired Student’s t test was used to compare populations. Averaged data presented as mean ± SEM, $p < 0.05$ (Student’s t test). Additional specifics to particular techniques are given below.

RT-qPCR—After completing each real-time PCR run, outlier C_t values among each triplicate were identified and excluded manually using the Q-test. Individual ΔΔCt values were calculated as the difference between ΔCt (Experimental or Control) and the average ΔCt (Control) value; ΔCt is the difference between averaged triplicate Ct values of the GOI and averaged triplicate Ct values of the reference gene. ΔΔCt values were used to calculate

$2^{-\Delta\Delta ct}$ values, which represent relative fold-changes of the GOI in the experimental group relative to the GOI in the control group.

Electrophysiology—Analysis and presentation software used for electrophysiological data include: Mini Analysis (Synaptosoft, Inc.), Origin (Microcal Software), GraphPad Prism (GraphPad Software), and Photoshop (Adobe) and Illustrator (Adobe).

Immunostaining quantification—Brains from each independent experiment were imaged on the same day with the same settings using a Zeiss LSM 710 confocal microscope. Comparisons were only made between brains from the same coverslip. Equivalent summed Z stacks surrounding the anatomical regions containing prominent Dα7 immunoreactivity were generated. ROIs were generated around the central brain and total fluorescence was measured in ImageJ.

Supplementary Material

Refer to Web version on PubMed Central for supplementary material.

ACKNOWLEDGMENTS

We thank Dr. Paul Salvaterra for the *Cha*^{ts} alleles, Dr. Mark Frye for the *UAS-TnT* line, Dr. Steven Sigrist for the *UAS-Dα7-EGFP* line, and Dr. Hugo Bellen for the *Dα7*$^{P\Delta EY6}$ and *Dα7-GAL4* lines and the Dα7 antibody. This work was funded by the National Institutes of Health R01GM08335 (S.T.).

REFERENCES

Albuquerque EX, Pereira EF, Alkondon M, and Rogers SW (2009). Mammalian nicotinic acetylcholine receptors: from structure to function. Physiol. Rev 89, 73–120. [PubMed: 19126755]

Amberg GC, Rossow CF, Navedo MF, and Santana LF (2004). NFATc3 regulates Kv2.1 expression in arterial smooth muscle. J. Biol. Chem 279, 47326–47334. [PubMed: 15322114]

Bischof J, Björklund M, Furger E, Schertel C, Taipale J, and Basler K (2013). A versatile platform for creating a comprehensive UAS-ORFeome library in Drosophila. Development 140, 2434–2442. [PubMed: 23637332]

Chen X, Yuan LL, Zhao C, Birnbaum SG, Frick A, Jung WE, Schwarz TL, Sweatt JD, and Johnston D (2006). Deletion of Kv4.2 gene eliminates dendritic A-type K+ current and enhances induction of long-term potentiation in hippocampal CA1 pyramidal neurons. J. Neurosci 26, 12143–12151. [PubMed: 17122039]

Daubert EA, and Condron BG (2007). A solid-phase immunostaining protocol for high-resolution imaging of delicate structures in the Drosophila larval central nervous system (CNS). CSH Protoc. 2007, pdb.prot4771.

Davis GW (2006). Homeostatic control of neural activity: from phenomenology to molecular design. Annu. Rev. Neurosci 29, 307–323. [PubMed: 16776588]

De Biasi M, and Dani JA (2011). Reward, addiction, withdrawal to nicotine. Annu. Rev. Neurosci 34, 105–130. [PubMed: 21438686]

Deitcher DL, Ueda A, Stewart BA, Burgess RW, Kidokoro Y, and Schwarz TL (1998). Distinct requirements for evoked and spontaneous release of neurotransmitter are revealed by mutations in the Drosophila gene neuronal-synaptobrevin. J. Neurosci 18, 2028–2039. [PubMed: 9482790]

DeKosky ST, Ikonomovic MD, Styren SD, Beckett L, Wisniewski S, Bennett DA, Cochran EJ, Kordower JH, and Mufson EJ (2002). Upregulation of choline acetyltransferase activity in hippocampus and frontal cortex of elderly subjects with mild cognitive impairment. Ann. Neurol 51, 145–155. [PubMed: 11835370]

Diao F, Waro G, and Tsunoda S (2009). Fast inactivation of Shal (K(v)4) K+ channels is regulated by the novel interactor SKIP3 in Drosophila neurons. Mol. Cell. Neurosci 42, 33–44. [PubMed: 19463952]

Diao F, Chaufty J, Waro G, and Tsunoda S (2010). SIDL interacts with the dendritic targeting motif of Shal (K(v)4) K+ channels in Drosophila. Mol. Cell. Neurosci 45, 75–83. [PubMed: 20550966]

Dineley KT, Westerman M, Bui D, Bell K, Ashe KH, and Sweatt JD (2001). Beta-amyloid activates the mitogen-activated protein kinase cascade via hippocampal alpha7 nicotinic acetylcholine receptors: In vitro and in vivo mechanisms related to Alzheimer's disease. J. Neurosci 21, 4125–4133. [PubMed: 11404397]

Duffy AM, Zhou P, Milner TA, and Pickel VM (2009). Spatial and intracellular relationships between the alpha7 nicotinic acetylcholine receptor and the vesicular acetylcholine transporter in the prefrontal cortex of rat and mouse. Neuroscience 161, 1091–1103. [PubMed: 19374941]

Fabian-Fine R, Skehel P, Errington ML, Davies HA, Sher E, Stewart MG, and Fine A (2001). Ultrastructural distribution of the alpha7 nicotinic acetylcholine receptor subunit in rat hippocampus. J. Neurosci 21, 7993–8003. [PubMed: 11588172]

Fayyazuddin A, Zaheer MA, Hiesinger PR, and Bellen HJ (2006). The nicotinic acetylcholine receptor Dalpha7 is required for an escape behavior in Drosophila. PLoS Biol. 4, e63. [PubMed: 16494528]

Fenster CP, Whitworth TL, Sheffield EB, Quick MW, and Lester RA (1999). Upregulation of surface alpha4beta2 nicotinic receptors is initiated by receptor desensitization after chronic exposure to nicotine. J. Neurosci 19, 4804–4814. [PubMed: 10366615]

Freeman A, Franciscovich A, Bowers M, Sandstrom DJ, and Sanyal S (2011). NFAT regulates pre-synaptic development and activity-dependent plasticity in Drosophila. Mol. Cell. Neurosci 46, 535–547. [PubMed: 21185939]

Frölich L (2002). The cholinergic pathology in Alzheimer's disease–discrepancies between clinical experience and pathophysiological findings. J. Neural Transm. (Vienna) 109, 1003–1013. [PubMed: 12111437]

Gilbert J, Shu S, Yang X, Lu Y, Zhu LQ, and Man HY (2016). β-Amyloid triggers aberrant over-scaling of homeostatic synaptic plasticity. Acta Neuropathol. Commun 4, 131. [PubMed: 27955702]

Gong N, Bodi I, Zobel C, Schwartz A, Molkentin JD, and Backx PH (2006). Calcineurin increases cardiac transient outward K+ currents via transcriptional up-regulation of Kv4.2 channel subunits. J. Biol. Chem 281, 38498–38506. [PubMed: 17060317]

Greenspan RJ, Finn JA Jr., and Hall JC (1980). Acetylcholinesterase mutants in Drosophila and their effects on the structure and function of the central nervous system. J. Comp. Neurol 189, 741–774. [PubMed: 6769980]

Gu S, Matta JA, Lord B, Harrington AW, Sutton SW, Davini WB, and Bredt DS (2016). Brain α7 Nicotinic Acetylcholine Receptor Assembly Requires NACHO. Neuron 89, 948–955. [PubMed: 26875622]

Hahm ET, Nagaraja RY, Waro G, and Tsunoda S (2018). Cholinergic Homeostatic Synaptic Plasticity Drives the Progression of Aβ-Induced Changes in Neural Activity. Cell Rep. 24, 342–354. [PubMed: 29996096]

Hall AM, Throesch BT, Buckingham SC, Markwardt SJ, Peng Y, Wang Q, Hoffman DA, and Roberson ED (2015). Tau-dependent Kv4.2 depletion and dendritic hyperexcitability in a mouse model of Alzheimer's disease. J. Neurosci 35, 6221–6230. [PubMed: 25878292]

Hernandez CM, Kayed R, Zheng H, Sweatt JD, and Dineley KT (2010). Loss of alpha7 nicotinic receptors enhances beta-amyloid oligomer accumulation, exacerbating early-stage cognitive decline and septohippocampal pathology in a mouse model of Alzheimer's disease. J. Neurosci 30, 2442–2453. [PubMed: 20164328]

Hussain A, Pooryasin A, Zhang M, Loschek LF, La Fortezza M, Friedrich AB, Blais CM, Üçpunar HK, Yépez VA, Lehmann M, et al. (2018). Inhibition of oxidative stress in cholinergic projection neurons fully rescues aging-associated olfactory circuit degeneration in Drosophila. eLife 7, e32018. [PubMed: 29345616]

Jang SS, and Chung HJ (2016). Emerging Link between Alzheimer's Disease and Homeostatic Synaptic Plasticity. Neural Plast. 2016, 7969272. [PubMed: 27019755]

Jones IW, and Wonnacott S (2004). Precise localization of alpha7 nicotinic acetylcholine receptors on glutamatergic axon terminals in the rat ventral tegmental area. J. Neurosci 24, 11244–11252. [PubMed: 15601930]

Jones IW, Barik J, O'Neill MJ, and Wonnacott S (2004). Alpha bungarotoxin-1.4 nm gold: a novel conjugate for visualising the precise subcellular distribution of alpha 7* nicotinic acetylcholine receptors. J. Neurosci. Methods 134, 65–74. [PubMed: 15102504]

Jung SC, and Hoffman DA (2009). Biphasic somatic A-type K channel downregulation mediates intrinsic plasticity in hippocampal CA1 pyramidal neurons. PLoS ONE 4, e6549. [PubMed: 19662093]

Keyser P, Borge-Renberg K, and Hultmark D (2007). The Drosophila NFAT homolog is involved in salt stress tolerance. Insect Biochem. Mol. Biol 37, 356–362. [PubMed: 17368199]

Kim J, Jung SC, Clemens AM, Petralia RS, and Hoffman DA (2007). Regulation of dendritic excitability by activity-dependent trafficking of the A-type K+ channel subunit Kv4.2 in hippocampal neurons. Neuron 54, 933–947. [PubMed: 17582333]

Kitamoto T, Xie X, Wu CF, and Salvaterra PM (2000). Isolation and characterization of mutants for the vesicular acetylcholine transporter gene in Drosophila melanogaster. J. Neurobiol 42, 161–171. [PubMed: 10640324]

Leiss F, Koper E, Hein I, Fouquet W, Lindner J, Sigrist S, and Tavosanis G (2009). Characterization of dendritic spines in the Drosophila central nervous system. Dev. Neurobiol 69, 221–234. [PubMed: 19160442]

Levy RB, and Aoki C (2002). Alpha7 nicotinic acetylcholine receptors occur at postsynaptic densities of AMPA receptor-positive and -negative excitatory synapses in rat sensory cortex. J. Neurosci 22, 5001–5015. [PubMed: 12077196]

Lubin M, Erisir A, and Aoki C (1999). Ultrastructural immunolocalization of the alpha 7 nAChR subunit in guinea pig medial prefrontal cortex. Ann. N Y Acad. Sci 868, 628–632. [PubMed: 10414345]

Macián F, López-Rodríguez C, and Rao A (2001). Partners in transcription: NFAT and AP-1. Oncogene 20, 2476–2489. [PubMed: 11402342]

Marder E, and Goaillard JM (2006). Variability, compensation and homeostasis in neuron and network function. Nat. Rev. Neurosci 7, 563–574. [PubMed: 16791145]

Masuyama K, Zhang Y, Rao Y, and Wang JW (2012). Mapping neural circuits with activity-dependent nuclear import of a transcription factor. J. Neurogenet 26, 89–102. [PubMed: 22236090]

Matta JA, Gu S, Davini WB, Lord B, Siuda ER, Harrington AW, and Bredt DS (2017). NACHO Mediates Nicotinic Acetylcholine Receptor Function throughout the Brain. Cell Rep. 19, 688–696. [PubMed: 28445721]

Mognol GP, Carneiro FR, Robbs BK, Faget DV, and Viola JP (2016). Cell cycle and apoptosis regulation by NFAT transcription factors: new roles for an old player. Cell Death Dis. 7, e2199. [PubMed: 27100893]

Nelson SB, and Turrigiano GG (2008). Strength through diversity. Neuron 60, 477–482. [PubMed: 18995822]

Nieves-Cintrón M, Amberg GC, Nichols CB, Molkentin JD, and Santana LF (2007). Activation of NFATc3 down-regulates the beta1 subunit of large conductance, calcium-activated K+ channels in arterial smooth muscle and contributes to hypertension. J. Biol. Chem 282, 3231–3240. [PubMed: 17148444]

Nordberg A (2001). Nicotinic receptor abnormalities of Alzheimer's disease: therapeutic implications. Biol. Psychiatry 49, 200–210. [PubMed: 11230871]

O'Dell KM, Armstrong JD, Yang MY, and Kaiser K (1995). Functional dissection of the Drosophila mushroom bodies by selective feminization of genetically defined subcompartments. Neuron 15, 55–61. [PubMed: 7619530]

Ortells MO, and Barrantes GE (2010). Tobacco addiction: a biochemical model of nicotine dependence. Med. Hypotheses 74, 884–894. [PubMed: 19962246]

Pakkanen JS, Jokitalo E, and Tuominen RK (2005). Up-regulation of beta2 and alpha7 subunit containing nicotinic acetylcholine receptors in mouse striatum at cellular level. Eur. J. Neurosci 21, 2681–2691. [PubMed: 15926916]

Picciotto MR, Addy NA, Mineur YS, and Brunzell DH (2008). It is not “either/or”: activation and desensitization of nicotinic acetylcholine receptors both contribute to behaviors related to nicotine addiction and mood. Prog. Neurobiol 84, 329–342. [PubMed: 18242816]

Ping Y, and Tsunoda S (2011). Inactivity-induced increase in nAChRs upregulates Shal K(+) channels to stabilize synaptic potentials. Nat. Neurosci 15, 90–97. [PubMed: 22081160]

Ping Y, Waro G, Licursi A, Smith S, Vo-Ba DA, and Tsunoda S (2011a). Shal/K(v)4 channels are required for maintaining excitability during repetitive firing and normal locomotion in Drosophila. PLoS ONE 6, e16043. [PubMed: 21264215]

Ping Y, Hahm ET, Waro G, Song Q, Vo-Ba DA, Licursi A, Bao H, Ganoe L, Finch K, and Tsunoda S (2015). Linking aβ42-induced hyperexcitability to neurodegeneration, learning and motor deficits, and a shorter lifespan in an Alzheimer’s model. PLoS Genet. 11, e1005025. [PubMed: 25774758]

Pozo K, and Goda Y (2010). Unraveling mechanisms of homeostatic synaptic plasticity. Neuron 66, 337–351. [PubMed: 20471348]

Pratt KG, Zimmerman EC, Cook DG, and Sullivan JM (2011). Presenilin 1 regulates homeostatic synaptic scaling through Akt signaling. Nat. Neurosci 14, 1112–1114. [PubMed: 21841774]

Raghu SV, Joesch M, Sigrist SJ, Borst A, and Reiff DF (2009). Synaptic organization of lobula plate tangential cells in Drosophila: Dalpha7 cholinergic receptors. J. Neurogenet 23, 200–209. [PubMed: 19306209]

Rao A, Luo C, and Hogan PG (1997). Transcription factors of the NFAT family: regulation and function. Annu. Rev. Immunol 15, 707–747. [PubMed: 9143705]

Rossow CF, Minami E, Chase EG, Murry CE, and Santana LF (2004). NFATc3-induced reductions in voltage-gated K+ currents after myocardial infarction. Circ. Res 94, 1340–1350. [PubMed: 15087419]

Rossow CF, Dilly KW, and Santana LF (2006). Differential calcineurin/NFATc3 activity contributes to the Ito transmural gradient in the mouse heart. Circ. Res 98, 1306–1313. [PubMed: 16614306]

Salvaterra PM, and McCaman RE (1985). Choline acetyltransferase and acetylcholine levels in Drosophila melanogaster: a study using two temperature-sensitive mutants. J. Neurosci 5, 903–910. [PubMed: 3920360]

Scala F, Fusco S, Ripoli C, Piacentini R, Li Puma DD, Spinelli M, Laezza F, Grassi C, and D’Ascenzo M (2015). Intraneuronal Aβ accumulation induces hippocampal neuron hyperexcitability through A-type K(+) current inhibition mediated by activation of caspases and GSK-3. Neurobiol. Aging 36, 886–900. [PubMed: 25541422]

Small DH (2004). Do acetylcholinesterase inhibitors boost synaptic scaling in Alzheimer’s disease? Trends Neurosci 27, 245–249. [PubMed: 15111005]

Small DH (2007). Neural network dysfunction in Alzheimer’s disease: a drug development perspective. Drug News Perspect. 20, 557–563. [PubMed: 18176660]

Small DH, and Fodero LR (2002). Cholinergic regulation of synaptic plasticity as a therapeutic target in Alzheimer’s disease. J. Alzheimers Dis 4, 349–355. [PubMed: 12446967]

Steinlein OK, and Bertrand D (2008). Neuronal nicotinic acetylcholine receptors: from the genetic analysis to neurological diseases. Biochem. Pharmacol 76, 1175–1183. [PubMed: 18691557]

Stocker RF, Heimbeck G, Gendre N, and de Belle JS (1997). Neuroblast ablation in Drosophila P[GAL4] lines reveals origins of olfactory interneurons. J. Neurobiol 32, 443–456. [PubMed: 9110257]

Sweeney ST, Broadie K, Keane J, Niemann H, and O’Kane CJ (1995). Targeted expression of tetanus toxin light chain in Drosophila specifically eliminates synaptic transmission and causes behavioral defects. Neuron 14, 341–351. [PubMed: 7857643]

Tsunoda S, and Salkoff L (1995a). Genetic analysis of Drosophila neurons: Shal, Shaw, and Shab encode most embryonic potassium currents. J. Neurosci 15, 1741–1754. [PubMed: 7891132]

Tsunoda S, and Salkoff L (1995b). The major delayed rectifier in both Drosophila neurons and muscle is encoded by Shab. J. Neurosci 15, 5209–5221. [PubMed: 7623146]

Turrigiano GG (2008). The self-tuning neuron: synaptic scaling of excitatory synapses. Cell 135, 422–435. [PubMed: 18984155]

Turrigiano G (2011). Too Many Cooks? Intrinsic and Synaptic Homeostatic Mechanisms in Cortical Circuit Refinement. Annu. Rev. Neurosci 34, 89–103. [PubMed: 21438687]

Wang X, McIntosh JM, and Rich MM (2018). Muscle Nicotinic Acetylcholine Receptors May Mediate Trans-Synaptic Signaling at the Mouse Neuromuscular Junction. J. Neurosci 38, 1725–1736. [PubMed: 29326174]

Yang MY, Armstrong JD, Vilinsky I, Strausfeld NJ, and Kaiser K (1995). Subdivision of the Drosophila mushroom bodies by enhancer-trap expression patterns. Neuron 15, 45–54. [PubMed: 7619529]

Yao JJ, Zhao QR, Liu DD, Chow CW, and Mei YA (2016). Neuritin Upregulates Kv4.2 α-Subunit of Potassium Channel Expression and Affects Neuronal Excitability by Regulating the Calcium-Calcineurin-NFATc4 Signaling Pathway. J. Biol. Chem 291, 17369–17381. [PubMed: 27307045]

Zhang J, and Shapiro MS (2012). Activity-dependent transcriptional regulation of M-Type (Kv7) K(+) channels by AKAP79/150-mediated NFAT actions. Neuron 76, 1133–1146. [PubMed: 23259949]

Highlights

- Inhibiting activity induces an increase in mEPSCs and Dα7 nAChR protein
- Inhibiting activity induces upregulation of K_v4/Shal mRNA, protein, and current
- Increasing Dα7 and/or NACHO is sufficient to induce upregulation of K_v4/Shal
- Inactivity-induced upregulation of *K_v4/Shal* requires transcription factor NFAT

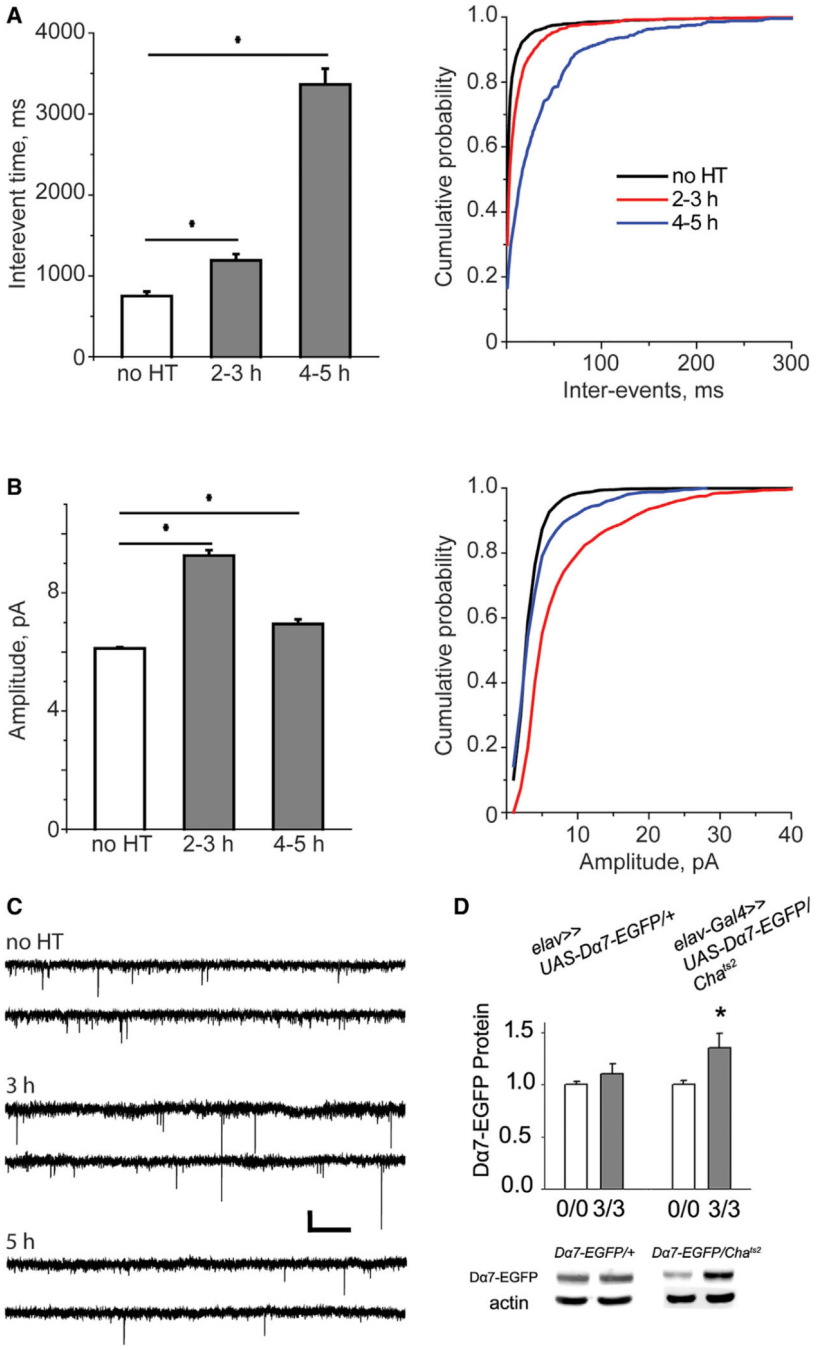

Figure 1. Inhibition of Cholinergic Activity in *Cha^{ts2}*/+ Neurons Induces a Homeostatic Increase in mEPSC Amplitudes and Dα7 Protein

(A–C) *Cha^{ts2}/+* primary cultures 8 DIV, grown at 18ºC, were heat treated (HT) at 30ºC for indicated times before mEPSCs were recorded. Comparisons are shown of mEPSC inter-event time (A) and amplitude (B) between *Cha^{ts2}/+* cultures without HT and *Cha^{ts2}/+* cultures with HT for indicated times. Note that mEPSCs from *Cha^{ts2}*/+ neurons show progressively decreased activity with significantly enhanced inter-event times with increasing HT (no HT, 750.19 ± 57.42 ms; 2/3 h HT, 1192.85 ± 76.34 ms; 4/5 h HT, 3364.76 ± 195.26 ms; N = 7–8 cells), and consequently, homeostatically enhanced amplitudes (no

HT, 6.12 ± 0.05 pA; 2/3 h HT, 9.26 ± 0.19 pA; 4/5 h HT, 6.95 ± 0.16 pA; N = 7–8 cells). (C) Representative traces showing synaptic activity from *Cha^{ts2}/+* control and experimental cells. Scale bars, 500 ms/5 pA.

(D) Quantification and representative immunoblots of *elav-Gal4>>UAS-Dα7-EGFP/+* and *elav-Gal4>>UAS-Dα7-EGFP/Cha^{ts2}* flies grown at 18ºC, then subjected to 0 or 3 h HT and 3 h recovery at 18ºC (0/0 or 3/3, respectively). All immunoblots were run with five heads per sample per lane. Anti-GFP band intensities were normalized to those of anti-actin, which were used as a loading control; for each condition. N = 24–46 samples per condition.

All data are presented as mean ± SEM; *p < 0.05, Student's t test.

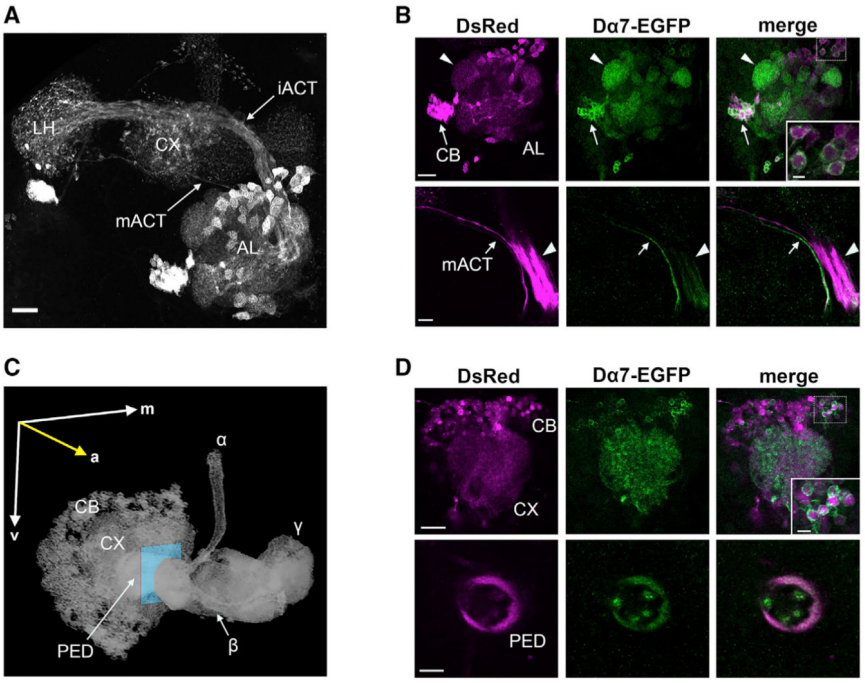

Figure 2. Dα7 nAChRs Are Localized to Somato-Dendritic and Axonal Compartments

Representative images showing Dα7-EGFP localization when *UAS-Dα7-EGFP* is driven by *GH146-Gal4* (A and B) or *201Y-Gal4* (C and D). DsRed and EGFP signals were enhanced with antibody labeling and are shown in magenta and green, respectively, in (B) and (D).

(A) Z-projection of confocal sections of the left side of an *GH146-Gal4>> UAS-DsRed* adult fly brain, showing the anatomy of the projection neurons (PNs; midline is right of image). Scale bar, 20 μm.

(B) Top: Z-projection of three confocal sections spanning 1 μm showing DsRed labeling of the PN cell bodies (CBs) (CB and arrows indicate an example cluster) and antennal lobe (AL) with example glomeruli indicated (arrowhead). Dα7-EGFP is clearly observed in PN CBs and in the glomeruli of the AL (center). Scale bar, 20 μm. Inset: a magnified view of the boxed region demonstrating membrane localization of Dα7-EGFP in CBs (scale bar, 5 μm). Bottom: Z-projection of three confocal sections spanning 1.5 μm showing DsRed (left) and Dα7-EGFP (center) localization on proximal axonal regions of the iACT (arrowhead) and mACT (arrow). Scale bar, 10 μm.

(C) 3D rendering of GFP signal in *201Y-Gal4>>UAS-mCD8-GFP* adult brains, demonstrating cellular compartments of the mushroom body. The blue plane indicates the approximate location of the cross-section shown in bottom row of (D). Image is rotated as indicated by the axes. m, medial; a, anterior; v, ventral.

(D) Top: Z-projection of three confocal sections spanning 3 μm through the CBs and calyx (CX) of the mushroom body (left). Dα7-EGFP is observed on CBs and within the neuropil of the CX (center). Scale bar, 20 μm. Inset: a magnified view of the boxed region demonstrating membrane localization of Dα7-EGFP in CBs (scale bar, 5 μm). Bottom: Single confocal cross-section of the peduncle (PED) showing DsRed (left) and Dα7-EGFP (center) localization on these axonal structures of the mushroom body. Scale bar, 10 μm. The

"despeckle" median noise filter in ImageJ was applied to all images shown from the GFP channel.

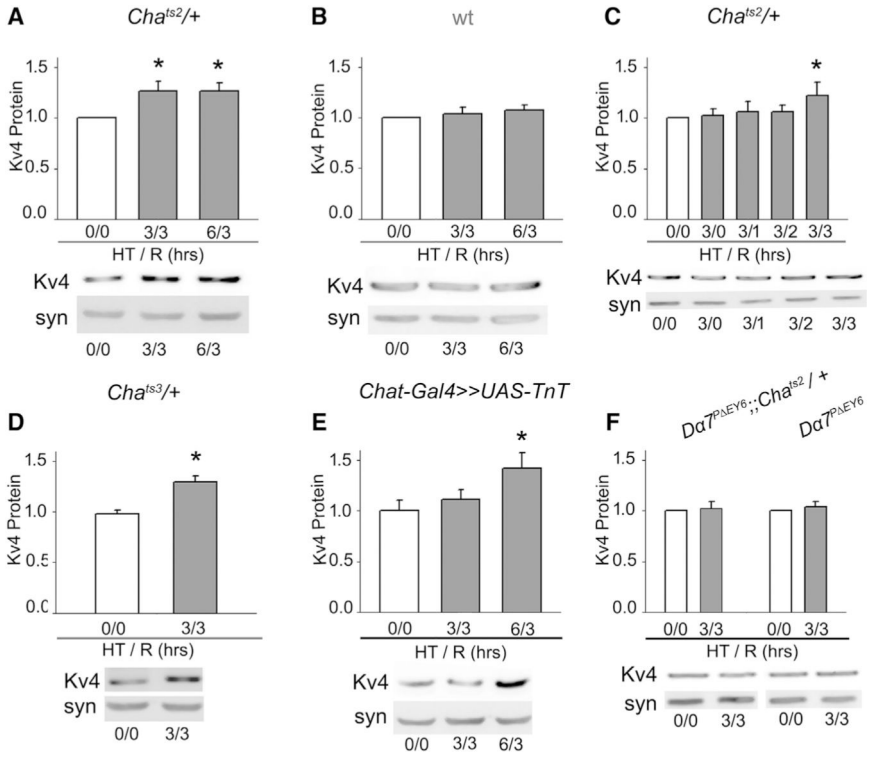

Figure 3. Blocking Neural Activity *In Vivo* Results in an Upregulation of K_V4/Shal Protein

(A–D) Quantification of relative K_V4/Shal protein levels and representative immunoblots from *Cha^{ts2}/+* (A and C), wild type (WT; B), and *Cha^{ts3}/+* (D) after HT protocols, indicated as hours of HT at 37ºC/h of recovery at 18ºC (e.g., 3/3, 6/3; 0/0 indicates flies kept at 18ºC with no HT). Note that 3–6 h HT of *Cha^{ts2}/+* induces an increase in K_V4/Shal protein.

(E) Quantification of relative K_V4/Shal protein levels and representative immunoblots from *ChaT-Gal4/tub-Gal80^{ts}>>UAS-TnT* flies after indicated HT shows a similar increase in K_V4/Shal levels after 6 h HT.

(F) Quantification and representative immunoblots of *Dα7^{PΔEY6};; Cha^{ts2}*/+, and *Dα7^{PΔEY6}* samples after indicated HT protocols show no significant change in K_V4/Shal in the absence of Dα7. All immunoblots were run with 5 male heads per lane; for each condition, number of samples (N) = 15–46. Anti-K_V4/Shal band intensities were normalized to those of anti-syntaxin (syn), which was used as a loading control.

Data are presented as mean ± SEM; *$p < 0.05$, Student's t test.

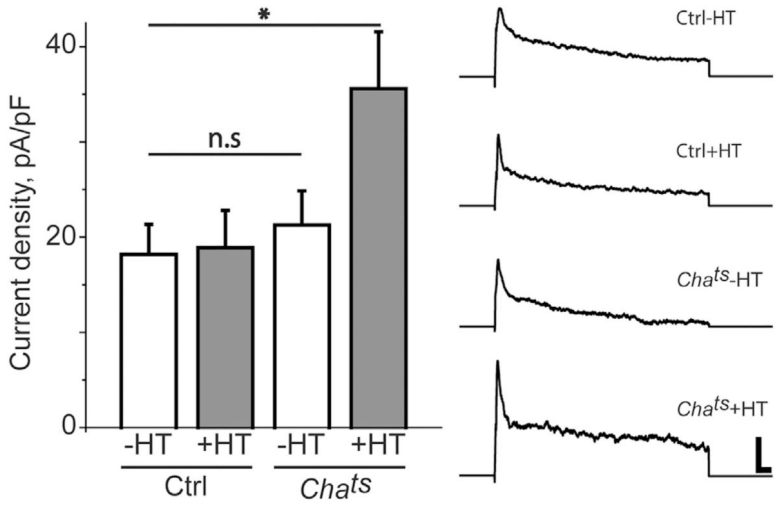

Figure 4. Inhibition of Cholinergic Activity in *Cha^{ts2}/+* Neurons Induces an Increase in K_V4/Shal Current Density

Primary cultures from genetic background controls (Ctrl) and *Cha^{ts2}/+* mutants (*Cha^{ts}*) were grown at 18ºC for 8 DIV, then either not HT (−HT) or HT for 6 h at 30ºC (+HT) followed by 2–3 h recovery at 18ºC. K_V4/Shal currents were separated from delayed rectifier currents as described in the text. Peak K_V4/Shal current densities were significantly increased in +HT *Cha^{ts2}/+* mutants compared to -HT *Cha^{ts2}/+* mutants or −HT and +HT controls (Ctrl−HT, 18.18 ± 3.15 pA/pF, N = 7; Ctrl+HT, 18.88 ± 3.93 pA/pF, N = 8; *Cha^{ts}*−HT, 21.26 ± 3.59 pA/pF, N = 14; *Cha^{ts}*+HT, 35.60 ± 5.99 pA/pF, N = 6). Data are presented as mean ± SEM; *$p < 0.05$, Student's t test. Scale bars, 100 pA/10 ms.

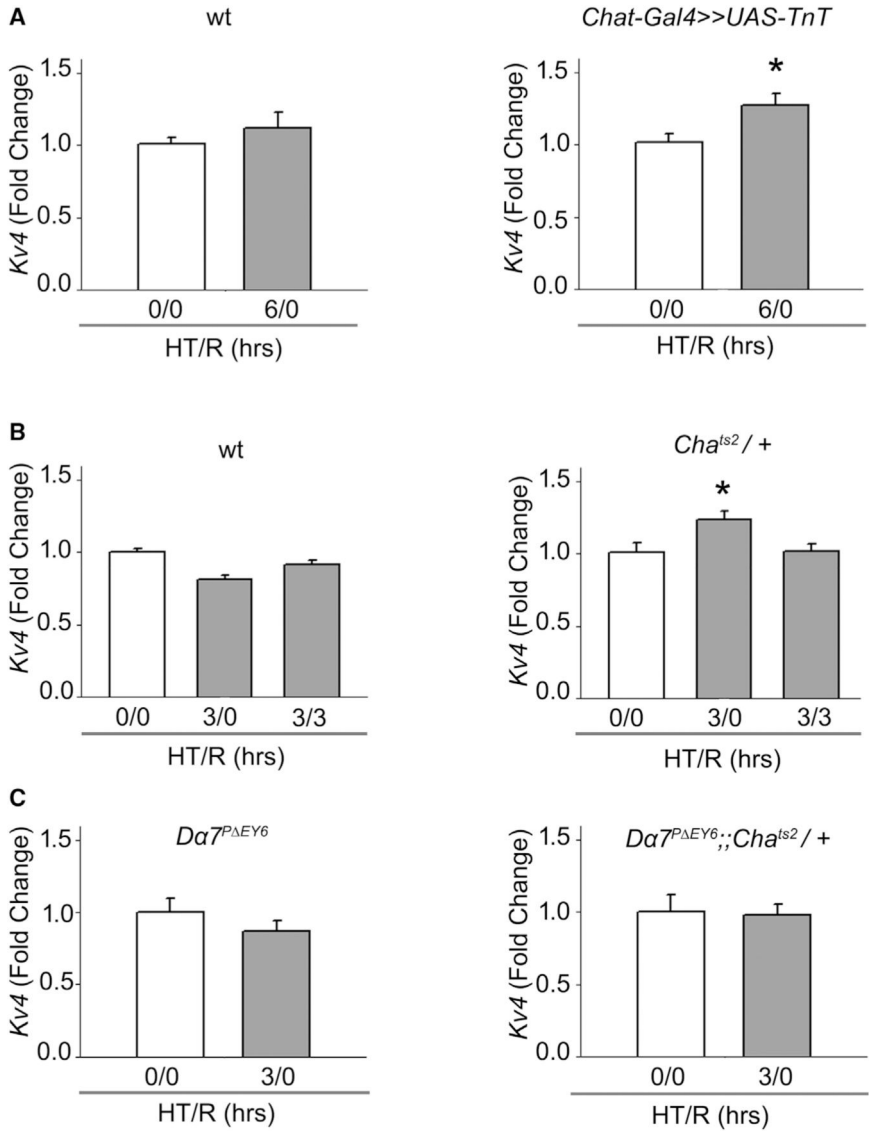

Figure 5. Blocking Neural Activity *In Vivo* Induces an Increase in K_V4/*Shal* mRNA, and This Increase Is Dependent on Dα7 nAChRs

qRT-PCR analyses of K_V4/*Shal* mRNA levels normalized to reference gene expression, expressed as "fold-change" (see Method Details for analyses and calculation).

(A) Comparison of WT and *Chat-Gal4>>UAS-TnT* male flies subjected to HT at 30ºC and recovery (HT/R; hours at 30ºC/h of recovery at 18ºC) protocols, as indicated. Note that 0/0 indicates no HT.

(B) Comparison of WT and Cha^{ts2}/+ flies subjected to HT/R protocols, as indicated.

(C) Comparisons of $D\alpha7^{P\Delta EY6}$ null mutants and $D\alpha7^{P\Delta EY6}$;; Cha^{ts2}/+ flies subjected to HT/R, as indicated.

Data are presented as mean fold-change ± SEM (means are from N = 10–17 independent RNA extraction and qRT-PCR); note that fold-changes are calculated in comparison to the corresponding 0/0 condition shown. *$p < 0.05$, Student's t test.

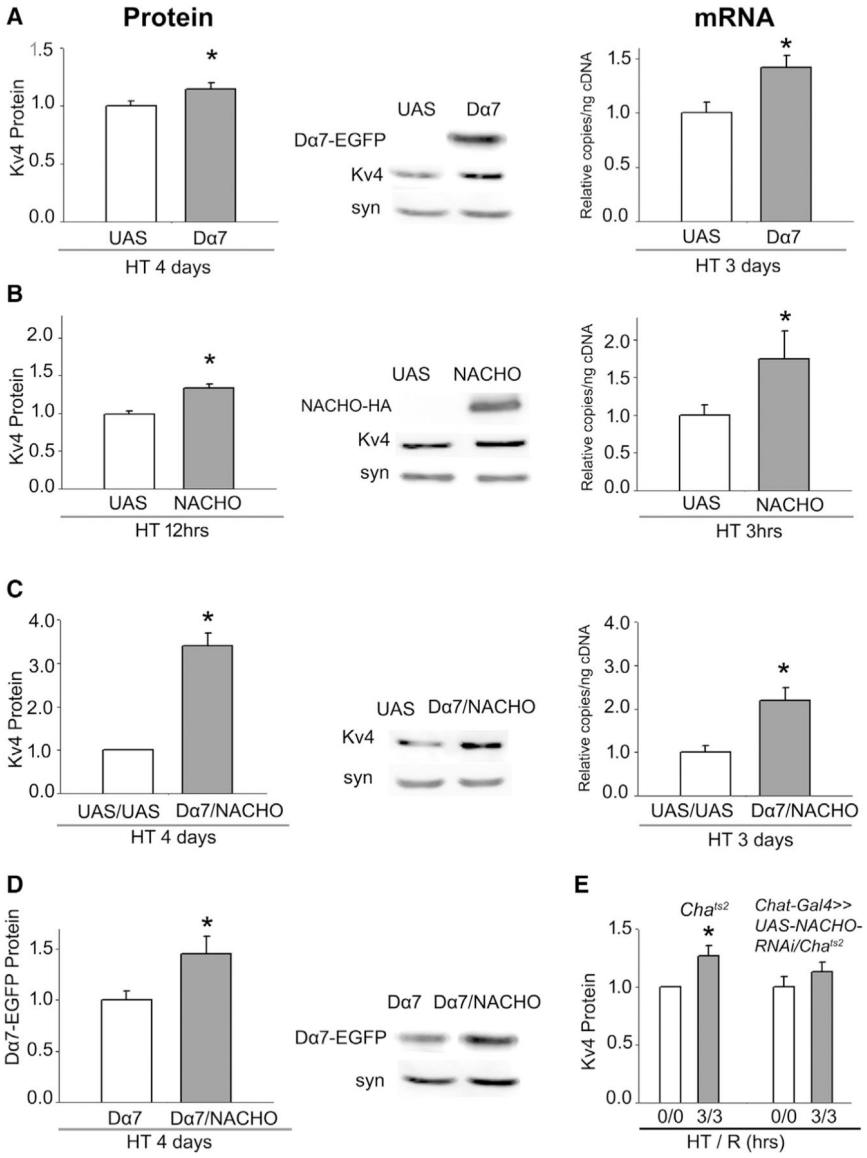

Figure 6. Increase in Dα7-EGFP and/or NACHO Is Sufficient to Induce an Increase in K_V4/Shal Protein and mRNA

(A–D) Representative immunoblots and quantitative analyses of steady-state protein levels (left) and digital droplet PCR (ddPCR) analyses (right) of samples from (A) *UAS-Dα7-EGFP/+* (UAS) and *elav-Gal4;tub-Gal80^{ts}>> UAS-Dα7-EGFP/+* (Dα7), (B) *UAS-NACHO-3xHA* (UAS) and *elav-Gal4;tub-Gal80^{ts}>>UAS-NACHO-3xHA* (NACHO), (C) *UAS-Dα7-EGFP/UAS-NACHO-3xHA* (UAS/UAS) and *elav-Gal4;tub-Gal80^{ts}>>UAS-Dα7-EGFP/UAS-NACHO-3xHA* (Dα7/NACHO), and (D) *elav-Gal4;-tub-Gal80^{ts}>>UAS-Dα7-EGFP/UAS-NACHO-3xHA* (Dα7/NACHO) and *elav-Gal4;tub-Gal80^{ts}>>UAS-Dα7-EGFP/UAS-NACHO-3xHA* (Dα7/NACHO). All fly lines were grown at 18ºC, allowing them to develop normally, then subjected to HT at 30ºC for the indicated times. All immunoblots (left) were run with five male heads per lane. Anti-K_V4/Shal or anti-GFP band intensities were normalized to those of anti-syntaxin (syn), which was used as a loading control. Experimental means were then normalized to similarly treated genetic background

control (UAS) means on the same immunoblots; for each condition, N = 17–23, data are represented as mean ± SEM; *p < 0.05, Student's t test. For ddPCR (right), data are presented as mean copy number per ng cDNA ± SEM (means are from N = 10–21 independent RNA extractions and RTs), normalized to mean copy number/ng cDNA from similarly treated genetic background control (UAS) values.

(E) Representative immunoblots and quantitative analyses of steady-state K_V4/Shal protein levels from heads of *Chat-Gal4/UAS-Dcr2>>UAS-NACHO-RNAi/Cha^{ts2}* (right; *Chat-Gal4>>UAS-NACHO-RNAi/Cha^{ts2}*) flies grown at 18ºC, then either not HT (0/0) or subjected to HT at 30ºC for 3 h followed by recovery at 18ºC for another 3 h (3/3). Immunoblot analyses are as described for (A)–(D); N = 15. Note that no significant increase in K_V4/Shal is observed when expression of NACHO is inhibited, in contrast to samples from similarly treated *Cha^{ts2}/+* flies (left; data here are the same as shown in Figure 3). *p < 0.05, Student's t test.

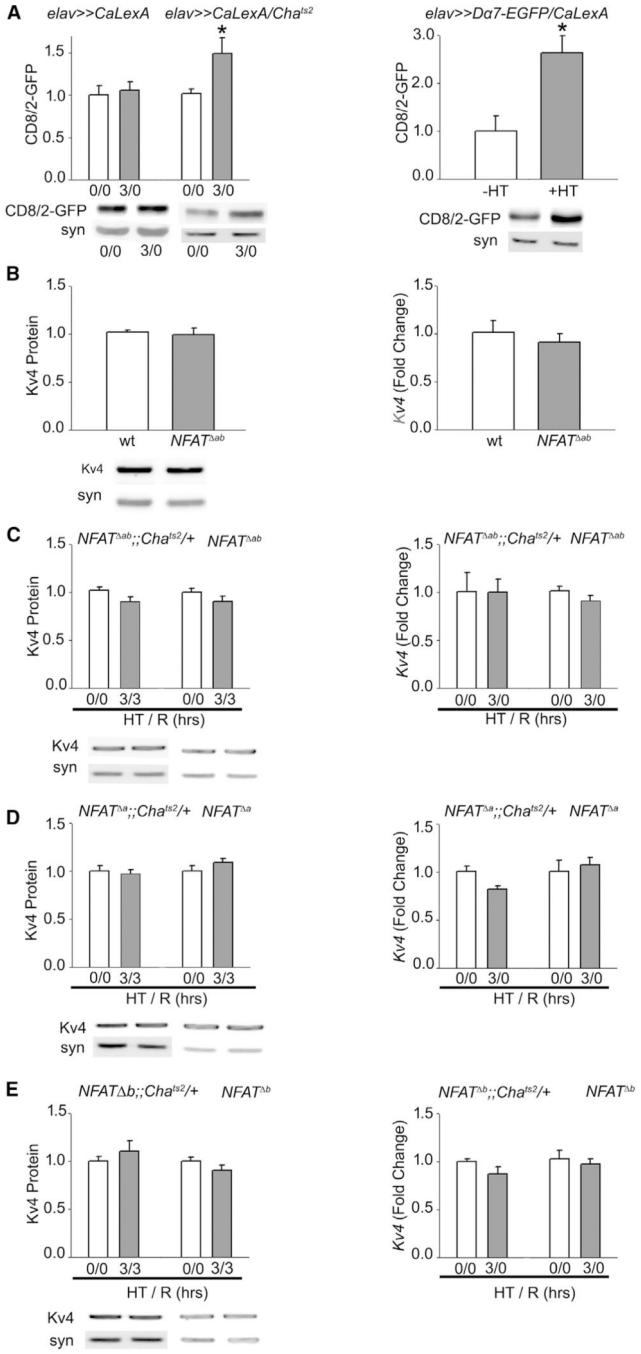

Figure 7. NFAT Is Required for the *Cha^{ts2}*-Induced Increase in K_V4/Shal Protein and mRNA

(A) Left: representative immunoblots and quantitative analyses for CD8/CD2-GFP expression in *elav-Gal4>>LexAop-CD8-GFP/+;UAS-mLexA-VP16-NFAT,LexAop-CD2-GFP/+* (*elav>>CaLexA*) and *elav-Gal4>>LexAop-CD8-GFP/+;UAS-mLexA-VP16-NFAT,LexAop-CD2-GFP/Cha^{ts2}* (*elav>>CaLexA/Cha^{ts2}*) flies subjected to 0/0 and 3/0 HT protocols (HT/R; hours at 30ºC/h of recovery at 18ºC), as indicated. Anti-GFP signals were normalized to anti-syntaxin (syn) signals as a loading control, then normalized to control (0/0) samples on the same immunoblots; N = 11–12 samples for *elav>>CaLexA*, N = 18 for

elav>>CaLexA/Cha^{ts2}. Note that the CD8/2-GFP levels responding to activation of the CaLexA reporter are elevated with HT of *Cha^{ts2}*. Right: representative immunoblots and quantitative analyses for CD8/CD2-GFP expression in heads from *elav-Gal4;tub-GAL80^{ts}>>UAS-mLexA-VP16-NFAT,LexAop-CD2-GFP/UAS-Dα7-EGFP; LexAop-CD8-GFP/+* flies were grown at 18ºC, then either not HT (−HT) or HT at 30ºC for 24 h (+HT). Quantification of GFP, normalized to anti-syntaxin, was performed as described above; N = 12–14 samples. Data are presented as mean +/− SEM. Note that the CD8/2-GFP levels responding to activation of the CaLexA reporter are elevated with HT to induce overexpression of Dα7-EGFP.

(B–E) Shown are representative immunoblots and quantitative analysis of relative K_V4/Shal protein levels (left) and qRT-PCR analyses for K_V4/Shal mRNA, expressed as fold-change (right) comparing (B) WT and *NFAT^{Δab}* mutants and (C) *NFAT^{Δab}* mutants and *NFAT^{Δab};;Cha^{ts2}/+*, (D) *NFAT^{Δa}* and *NFAT^{Δa};;Cha^{ts2}/+*, and (E) *NFAT^{Δb}* and *NFAT^{Δb};;Cha^{ts2}/+* lines, subjected to HT/R (hours at 30ºC/h of recovery at 18ºC) protocols, as indicated. All immunoblots were run with five heads per lane. Anti-K_V4/Shal or anti-GFP band intensities were normalized to those of anti-syntaxin (syn), which was used as a loading control; for each condition; N = 15–25; data are represented as mean ± SEM

For qRT-PCR, data are presented as mean fold-change ± SEM (means are from N = 9–14 independent RNA extraction and qRT-PCR); note that fold-changes are calculated in comparison to the corresponding 0/0 condition shown. *$p < 0.05$, Student's t test.

KEY RESOURCES TABLE

REAGENT or RESOURCE Antibodies	SOURCE	IDENTIFIER
Antibodies		
anti-Dα7	Dr. Hugo Bellen	(Fayyazuddin et al., 2006)
anti-K_v4/Shal	Dr. Susan Tsunoda	(Diao et al., 2009)
anti-actin	EMD Millipore	MAP1501
rabbit anti-GFP	Torrey Pines Biolabs	TP401; RRID:AB_10013661
anti-syntaxin	Developmental Hybridoma Studies Bank	8C3-S
anti-HA	Biolegend	901501; RRID:AB_2565006
chicken anti-GFP	Aves Labs	GFP-1020; RRID:AB_10000240
anti-RFP	Rockland Immunochemicals Inc.	600–401-379; RRID:AB_2209751
Chemicals, Peptides and Recombinant Proteins		
qRT-PCR Probe #66 for *Kv4/Shal* and *RPS20*	Universal Probe Library (UPL), Roche Molecular Systems	04688651001
qRT-PCR Probe #147 for *eIF1A*	Universal Probe Library (UPL), Roche Molecular Systems	04694333001
Experimental Models: Organisms/Strains		
w^{1118}	Bloomington Drosophila Stock Center	FlyBase: FBal0018186
UAS-TnT	Dr. Mark Frye	(Deitcher et al., 1998; Sweeney et al., 1995)
Cha^{ts} alleles	Dr. Paul Salvaterra	(Salvaterra and McCaman, 1985)
UAS-Dα7-EGFP	Dr. Steven Sigrist	(Leiss et al., 2009)
$Dα7^{PΔEY6}$	Dr. Hugo Bellen	(Fayyazuddin et al., 2006)
Dα7-GAL4	Dr. Hugo Bellen	(Fayyazuddin et al., 2006)
UAS-NACHO-3xHA	FlyORF	FlyORF: F002996 (Bischof et al., 2013)
UAS-mLexA-VP16-NFAT, LexAop-CD8-GFP, LexAop-CD2-GFP	Bloomington Drosophila Stock Center	BDSC: 66542 (Masuyama et al., 2012)
$NFAT^{ΔAB}$, $NFAT^{ΔA}$, and $NFAT^{ΔB}$ alleles	Bloomington Drosophila Stock Center	BDSC: 32652, 33593, 36269 (Keyser et al., 2007)
$elav\text{-}GAL4^{c155}$	Bloomington Drosophila Stock Center	BDSC: 458
201Y-GAL4	Bloomington Drosophila Stock Center	BDSC: 4440 (O'Dell et al., 1995; Yang et al., 1995)
GH146-GAL4	Bloomington Drosophila Stock Center	BDSC: 30026 (Stocker et al., 1997)
UAS-RNAi-NACHO	Vienna Drosophila Resource Center	VDRC: 46993
Oligonucleotides		
Kv4/Shal primers (*Left*, GCTAACGAAAGGAGGAACG; *Right*, TGAACTTATTGCTGTCATTTTGC)	This paper	N/A
RPS20 primers (*Left*, CGACCAGGGAAATTGCTAAA; *Right*, CGACATGGGGCTTCTCAATA)	This paper	N/A
eIF1A primers (*Left*, TCG TCT GGA GGC AAT GTG; *Right*, GCC CTG GTT AAT CCA CAC C)	This paper	N/A

REAGENT or RESOURCE Antibodies	**SOURCE**	**IDENTIFIER**
Software and Algorithms		
pClamp10	Molecular Devices Corp	N/A
ImageJ	Open Source	https://imagej.net/
Mini Analysis	Synaptosoft, Inc.	N/A
Origin	Microcal Software	N/A
GraphPad Prism	GraphPad Software	N/A
Photoshop	Adobe	N/A
Illustrator	Adobe	N/A